PHILOSOPHICAL TRANSACTIONS OF THE ROYAL SOCIETY A

Phil. Trans. R. Soc. A (2010) **368**, 1405–1453
doi:10.1098/rsta.2009.0275

Review

On the application potential of gold nanoparticles in nanoelectronics and biomedicine

By Melanie Homberger and Ulrich Simon*

Institute of Inorganic Chemistry and JARA-FIT, RWTH Aachen University, Landoltweg 1, 52074 Aachen, Germany

Ligand-stabilized gold nanoparticles (AuNPs) are of high interest to research dedicated to future technologies such as nanoelectronics or biomedical applications. This research interest arises from the unique size-dependent properties such as surface plasmon resonance or Coulomb charging effects. It is shown here how the unique properties of individual AuNPs and AuNP assemblies can be used to create new functional materials for applications in a *technical* or *biological* environment. While the term *technical environment* focuses on the potential use of AuNPs as subunits in nanoelectronic devices, the term *biological environment* addresses issues of toxicity and novel concepts of controlling biomolecular reactions on the surface of AuNPs.

Keywords: gold cluster; nanoelectronics; single-electron tunnelling; cytotoxicity; biomedical applications; assembly principles

1. Introduction

Ligand-stabilized gold nanoparticles (AuNPs) in the size range of a few nanometres are objectives of high interest to research dedicated to future technologies such as sensor applications (Franke *et al.* 2006; Jumar Ahirawal & Mitra 2009; Zhang *et al.* 2009), medical diagnostics (Wilson 2008), catalysis (Corma & Garcia 2008; Pina *et al.* 2008) or nanoelectronics (Schmid & Simon 2005; Schmid 2008). This extraordinary interest is reflected by the enormous increase in original works published as well as by the large number of reviews dealing with the preparation, electronic structure and optical properties in combination with the potential applications of AuNPs (Daniel & Astruc 2004; Eustis & El-Sayed 2006; Grzelczak *et al.* 2008; Murray 2008). The widespread and highly interdisciplinary field of these research activities relies on features of metal nanoparticles in general and AuNPs in particular.

AuNPs, in particular, exhibit good chemical stability. In principle, they can be surface functionalized with almost every type of electron-donating molecule including biomolecules (Daniel & Astruc 2004; Wilton-Ely 2008). Beyond that,

*Author for correspondence (ulrich.simon@ac.rwth-aachen.de).

One contribution of 13 to a Theme Issue 'Metal clusters and nanoparticles'.

in the meantime, several protocols have been developed that allow their assembly into one, two and three dimensions (Daniel & Astruc 2004; Schmid & Simon 2005; Ofir *et al.* 2008; Park *et al.* 2008). Altogether, these facts triggered the development of concepts for the design of novel materials with very specific properties based on the unique size-dependent properties of single nanoparticles and their collective properties in assemblies, owing to dipolar, magnetic or electronic coupling.

Some of the unique characteristics of metal nanoparticles in general are already apparent just by looking at the melting point behaviour when reducing the size of the bulk metal down to an aggregate size of a few nanometres. For example, bulk gold has a melting point of around 1064°C (Lide 1995), and it is defined as an elemental specific property (Brune *et al.* 2006). Upon reducing the size of a respective piece of metal under investigation, the melting point drops continuously and AuNPs with a size of approximately 2 nm exhibit a melting point of around 200°C (Buffat & Borel 1976; Castro *et al.* 1990). This lower melting point can be attributed to the increasing ratio of surface atoms to inner atoms upon decreasing the particle size. The surface atoms have a lower coordination number and are therefore more mobile. Thus, the melting point reflects the onset of atomic mobility comparable to that in the melted state. This means that, in principle, it could even be possible to reach a melting point of 'gold' which is close to room temperature.

Further characteristic properties become evident by studying the optical properties. For example, an aqueous dispersion of colloidal gold (in the size range of approx. 15–100 nm) appears ruby red in transmitted light (Daniel & Astruc 2004). This effect arises from the surface plasmon resonance (SPR) excitation, which is based on the interaction with the electromagnetic field of the incoming light resulting in a collective oscillation of the conduction electrons on the nanoparticle's surface. The light thereby creates surface polarization charges, which act as a restoring force on the electron gas and thus induce oscillation of the electron plasma. The SPR for small AuNPs appears in the visible and near-infrared range domains of light, whereas its position is influenced by the size, shape and the surrounding media of the single nanoparticle, including the nature of the ligand shell and the interparticle distances in dispersions (Myroshnychenko *et al.* 2008; Pecharromán *et al.* 2008). For example, investigations of gold colloid dispersions in SiO_2 matrices under volume ratio control revealed that, upon reducing the interparticle distance, the single AuNPs start to 'feel' each other; this is observable in a typical redshift of the plasmon resonance, which is visually observable by a colour change from red to blue. This unique characteristic triggered ideas for the fabrication of hybrid materials with controllable optical properties (Ung *et al.* 2002; Hu *et al.* 2006; Sendrouiu *et al.* 2006; Chen *et al.* 2008).

Upon reducing the size of bulk gold, an additional aspect of fundamental relevance is revealed: the electrical properties. Single nanoparticles with sizes in the range of a few nanometres exhibit an electronic structure that corresponds to an intermediate electronic structure between the band structure of the bulk metal and the discrete energy levels of molecules with a characteristic highest occupied molecular orbital (HOMO)–lowest unoccupied molecular orbital (LUMO) gap.

In the size range of approximately 2 nm and below, single particles can be considered as quantum dots (Halperin 1986). A thoroughly studied example is the so-called 'Schmid cluster', $Au_{55}(PPh_3)_{12}Cl_6$ ('Au_{55}'), with a core size of 1.4 nm. Since its discovery (Schmid *et al.* 1981), the cluster has been intensively investigated and an excellent overview about this compound has recently been presented by Schmid (2008). Impedance spectroscopy (IS), voltammetric and scanning tunnelling spectroscopy (STS) investigations revealed Coulomb charging at room temperature. This fact shows that this cluster is a promising subunit in nanoelectronic devices using the so-called Coulomb blockade and the controlled tunnelling of individual charges, i.e. single-electron tunnelling (SET). Furthermore, low-temperature STS investigations gave clear evidence of discrete energy levels (Zhang *et al.* 2003). Generally, the level spacing, as well as the position of the Coulomb gap in small metal clusters, is also influenced by the size, shape and the surrounding medium, including the ligand shell and the interparticle distances (Remacle & Levine 2001).

With respect to biological applications, another crucial aspect of AuNP has recently moved into focus: the potential cytotoxicity. Since early investigations of triphenylmonosulphonate-stabilized 1.4 nm Au nanoparticles, i.e. the water-soluble derivative of Au_{55}, revealed an even higher toxicity than *cisplatin*, as demonstrated for different cell lines (Tsoli *et al.* 2005), the key question is which parameters influence the impact of AuNPs on the viability of cells, i.e. for intracellular gene regulation (Rosi *et al.* 2006), chemotherapy (Podsiadlo *et al.* 2008) or drug delivery (Han *et al.* 2007*a*,*b*), and consequently the number of publications dedicated to toxicity has increased drastically (Connor *et al.* 2005; Nel *et al.* 2006; Pan *et al.* 2007; Boisselier & Astruc 2009; El-Ansary & Al-Daihan 2009).

Having the above-mentioned different properties of AuNPs in mind, this review aims at presenting a topical overview on how the unique properties of individual AuNPs and AuNP assemblies can be used to create new functional materials for applications in a *technical* or *biological environment*. With the term *technical environment*, we focus on the potential use of AuNPs as subunits in nanoelectronic devices. The term *biological environment* addresses issues of toxicity and novel concepts of controlling biomolecular reactions on the surface of AuNPs, which appeared as a very recent focus in potential biomedical applications. The review will not provide an overview of the variety of concepts involved in diagnostics, imaging or labelling. Hence, we will cover the basic principles of AuNP preparation, SET on ligand-stabilized AuNPs, nanoparticle assemblies and electrical addressing. Furthermore, parameters eliciting the cytotoxicity of AuNPs and concepts of detecting and triggering biomolecular reactions on the surface of AuNPs will be presented. Since these research topics represent rapidly growing fields of research, this review can highlight only selected recent developments, while having an emphasis on research performed in our group.

2. Preparation of AuNPs

Many protocols have been developed for the preparation of different types of AuNPs, varying in size, shape and ligand shell composition. However, owing to the multiple control parameters, the preparation of a distinct nanoparticle type still

represents a great challenge reflected by a great number of publications dedicated to this topic (Pileni 2003, 2007; Schmid 2004; Burda *et al.* 2005; Richards *et al.* 2005; Grzelczak *et al.* 2008). Very comprehensive and extended overviews are given by Daniel & Astruc (2004) and by Grzelczak *et al.* (2008).

In order to use the size-dependent properties of metal nanoparticles, ideally monodisperse nanoparticles are required. The typical procedures yielding ligand-stabilized AuNPs always involve some kind of dispersity, which means that, with respect to applications, sophisticated size separation techniques are necessary to reduce the size distribution. This presumption of ideal monodispersity is realized in gold clusters consisting of a defined number of atoms. In the following, the basic principles of ligand-stabilized AuNPs and Au cluster preparation will be summarized briefly.

(*a*) *Ligand-protected AuNPs*

The overall basic synthesis principle is the reduction of metal salts via suitable reducing agents in the presence of ligand molecules, which form self-assembled (SA) monolayers on the nanoparticle surface and thus stabilize the nanoparticles. Besides the well-known citrate-stabilized AuNPs (refer to Turkevich *et al.* 1951; Love *et al.* 2005), typical ligand molecules for AuNPs are phosphines, amines and thiolates, of which the thiolates are most intensively investigated owing to the strong binding characteristic of thiol to gold compared with phosphines and amines and the predominantly electrostatically bound citrate.

Typical reducing agents used in the direct reduction route are citrate and sodium borohydride. The latter is applied most frequently since Brust *et al.* (1994) introduced a two-phase liquid–liquid preparation method in which $AuCl_4^-$ is transferred from the aqueous solution to toluene using tetraoctylammonium bromide as a phase-transfer agent and reduced with aqueous sodium borohydride in the presence of an alkane thiol, yielding stable nanoparticles with small size distributions, ranging from 1 to 3 nm. In this case, the control over the particle size is achieved by varying the thiol/gold salt ratio and the addition rate of sodium borohydride. The respective nanoparticles can be precipitated, re-dissolved, chromatographed and further surface-modified without any apparent change in properties. Brust *et al.* (1995) developed this reaction route to a one-phase system also, which allows working without a phase-transfer agent and thus avoids the phase-transfer step and eventually further purification from tetraoctylammonium bromide impurities.

However, one disadvantage of sodium borohydride is its strong reducing character, which restricts this route to non-functionalized ligands. An alternative much milder reducing agent in this context was recently demonstrated by Sardar & Shumaker-Parry (2009). They prepared various AuNPs by using borabicyclo-[3.3.1]nonane (9-BBN), with sizes around 2 nm. This reducing agent allows the use of functionalized alkanethiols such as 11-mercaptoundecanoic acid and 11-mercapto-1-undecanoic and azide-terminated undecyl disulphide, within a direct one-phase reduction route.

A method that also allows the direct implementation of ligands that are typically not stable within the sodium borohydride route is the surfactant-free synthesis of AuNPs by Schulz-Dobrick *et al.* (2005). In this approach, $HAuCl_4$ solved in diethyleneglycol dimethyl ether (diglyme) is reduced by sodium

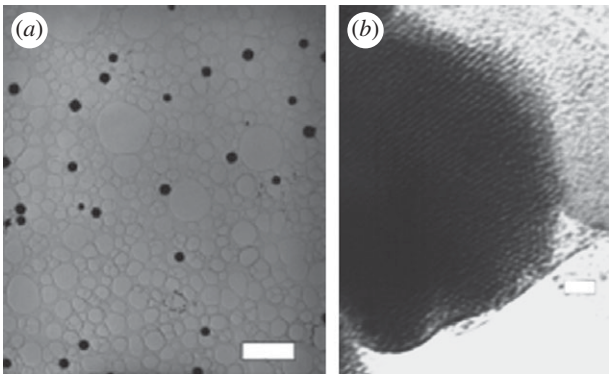

Figure 1. (*a*) Microcrystals of $Au_{55}(PPh_3)_{12}Cl_6$ and (*b*) high-resolution image of a thin crystal part indicating the highly ordered cluster layers. Reproduced with permission from Schmid *et al.* (1999). Copyright © The Royal Society of Chemistry. Scale bar, (*a*) 5 µm; (*b*) 20 µm.

naphthalenide in diglyme. The formed AuNPs in this first step are just weakly solvent-molecule protected and can be further stabilized and functionalized by simply adding respective ligand molecules (1-dodecanethiol, dodecanamine, oleylamine and triphenylphosphine (TPP) sulphide). Furthermore, this approach allows the size of the nanoparticles to be tuned within the range 1.9–5.2 nm, depending on the volume of the added reduction solution and the time between the addition of reduction solution and the addition of ligand molecule solution.

Besides the choice of the ligand and the reaction condition, the question is still how to gain reproducible good control over the particle size distribution. In this context, an approach that uses tailor-made multidentate polythioether ligands during nanoparticle formation was introduced recently. The basic idea is that a large multidentate ligand structure might favour well-defined particle sizes by enwrapping the whole particle. Thereby, AuNPs of approximately 2 nm are formed in a two-phase water/dichloromethane system, closely following the procedure developed by Brust *et al.* (1994). This concept is promising as it would allow control of the number and topology of functional groups on the particle surface (Peterle *et al.* 2008).

(*b*) *Gold clusters*

Gold clusters of defined composition have been known for several years. Among these, the $Au_{55}(PPh_3)_{12}Cl_6$ cluster introduced by Schmid *et al.* (1981) is probably the most intensively studied owing to the quantum size behaviour, which reflects the properties of a metallic quantum dot, as already mentioned in §1 (Simon *et al.* 1993*a*,*b*; Schmid 1998). The preparation protocol of $Au_{55}(PPh_3)_{12}Cl_6$ follows the direct reduction of the Au(I) complex, $Au(PPh_3)Cl$, solved in benzene with *in situ* formed B_2H_6 as the reducing agent. The cluster may be isolated as a microcrystalline dark brown solid, best soluble in dichloromethane (figure 1) (Schmid *et al.* 1999).

Profound investigations involving transmission electron microscopy (TEM), small-angle X-ray diffraction of microcrystals and ^{31}P-NMR experiments have been performed to determine the structural characteristics and stability

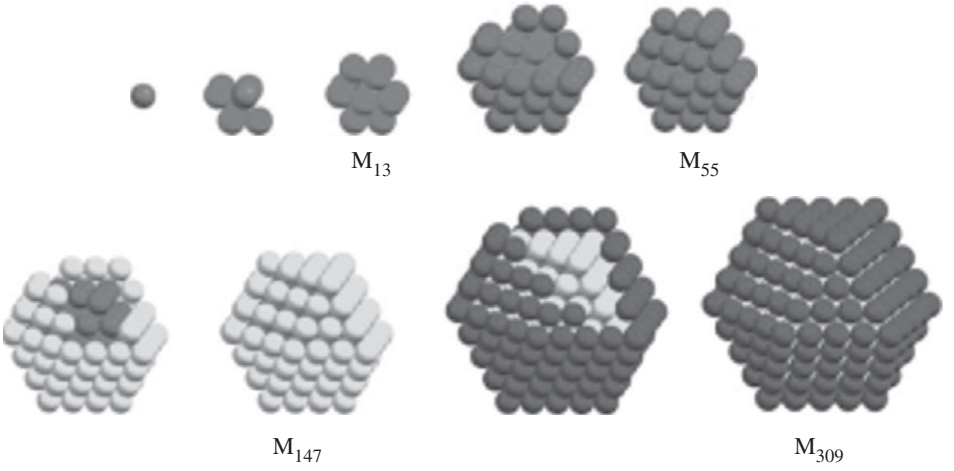

Figure 2. Organization of full-shell clusters. The first single atom is surrounded by 12 others to give a one-shell cluster M_{13}. Forty-two atoms can be densely packed on the 12 atoms ending with the M_{55} two-shell cluster, followed by 92 atoms and 162 atoms to give M_{147} and M_{309}, respectively. Adapted from Schmid (2008). Copyright © The Royal Society of Chemistry.

(Schmid 1985, 2008; Schmid *et al.* 1999). At this point, we would just like to mention that ^{31}P-NMR experiments showed that the phosphine ligands partially dissociate in the solution, leading to the formation of cluster aggregates. Therefore, solutions of the cluster reveal no long-term stability, although they are stable for at least hours.

The defined stoichiometrical composition of $Au_{55}(PPh_3)_{12}Cl_6$ refers to the so-called full-shell cluster model, in which the cluster is considered as a cut-out of the bulk lattice structure, implying that the cluster consists of a metal nucleus surrounded by shells of closely packed metal atoms, each shell having $10n^2+2$ atoms, where n is the number of shells (Schmid *et al.* 1990; Schmid 2004). The Au_{55} cluster therefore represents an example of a two-shell cluster (figure 2).

With a recently published theoretical investigation on ligand and solvation effects on the electronic properties of the Au_{55} cluster, Periyasamy & Remacle (2009) provided an optimized geometry model based on discrete Fourier transform calculations for the Au_{55} cluster. The calculations are in agreement with the above-described structure model of an icosahedral cluster core geometry derived from the full-shell cluster principle. This concept still holds true when comparing bare Au_{55} and ligated Au_{55} clusters ($Au_{55}(PH_3)_{12}$, $Au_{55}(PH_3)_{12}Cl_6$ and $Au_{55}(PH_3)_{12}Cl_6$ $54H_2O$) (figure 3). The phosphine ligands coordinate to the face edge atom of the cluster, and the six Cl atoms are asymmetrically coordinated to the three face-centred gold atoms. The calculated diameters based on these geometries are in agreement with the previously performed experimental findings (Periyasamy & Remacle 2009). Furthermore, with these studies, they provided an approach to understand how ligand and solvation effects influence the electrical properties of the Au_{55} cluster. For example, for the case of $Au_{55}(PH_3)_{12}Cl_6$, a strong coordination of the Cl ligands with the Au atoms of the outer shell was determined, reflected by an increase of 1.5 eV in the charging energy when compared with the bare Au_{55} clusters. In the case of $Au_{55}(PH_3)_{12}Cl_6$ modelled

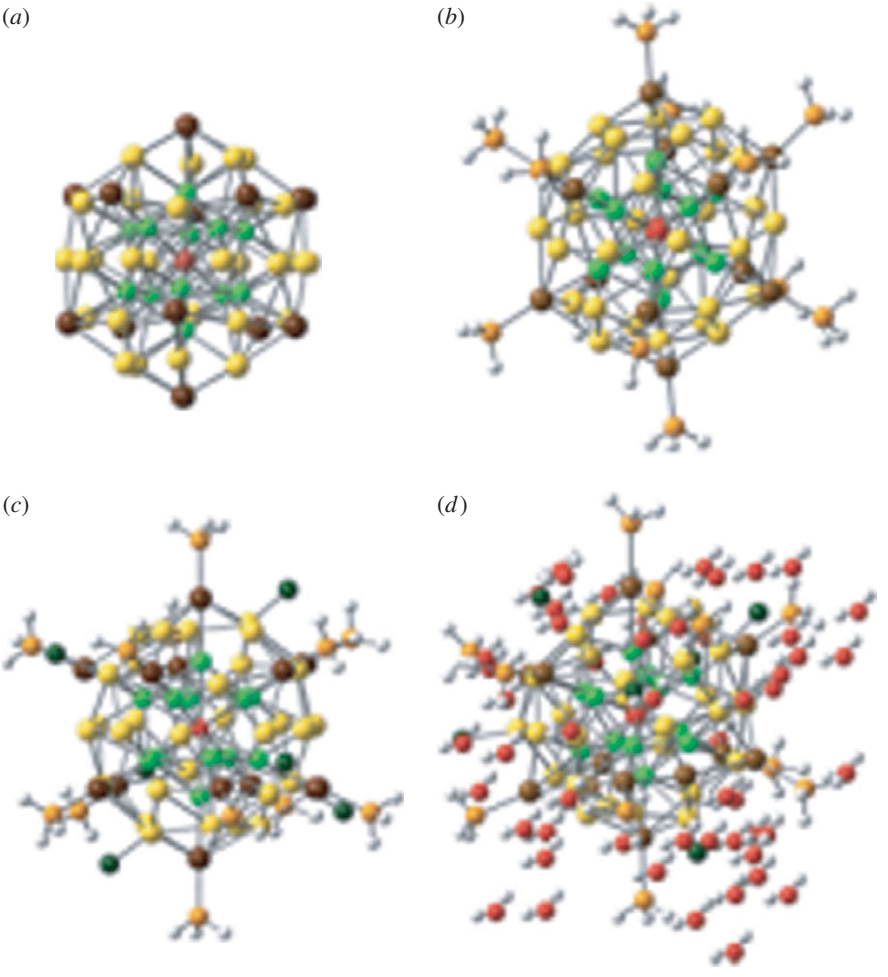

Figure 3. Optimized geometry of the stable isomers of (*a*) Au_{55}, (*b*) $Au_{55}(PH_3)_{12}$, (*c*) $Au_{55}(PH_3)_{12}Cl_6$ and (*d*) $Au_{55}(PH_3)_{12}Cl_6$ $54H_2O$. All clusters exhibit a distorted icosahedral geometry where a central Au (red) is surrounded by two shells. A first shell of 12 Au (green) in a sphere of approximately 0.29 nm and a second shell of 42 Au, the 12 face edge atoms (brown) being at approximately 0.58 nm and the 30 face-centred ones (yellow) at approximately 0.51 nm from the central gold atom, respectively. Reprinted with permission from Periyasamy & Remacle (2009). Copyright © 2009 American Chemical Society.

with $54H_2O$, a decrease in the charging energy of approximately 2 eV down to 1 eV (compared with 3.5 eV for the bare Au_{55} cluster) was calculated, which the authors ascribe to a weakening of the Cl–Au bond owing to the fact that the H_2O affects primarily the Cl coordination to the Au_{55} cluster by H-bonding.

Examples of one-shell clusters displaying the theoretically predicted icosahedral structure concept as depicted in figure 2 are $[Au_{13}(dppm)_6(NO_3)_4]$ (dppm = $Ph_2CH_2CH_2PPh_2$) (van der Velden *et al.* 1981*a*) and $[Au_{13}(PMe_2Ph)_{10}Cl_2](PF_6)_3$ (Briant *et al.* 1981). The cluster $[Au_{13}(dppm)_6(NO_3)_4]$ is synthesized by the reduction of $Au_2(dppm)(NO_3)_2$ with $NaBH_4$. The chelating dppm molecules trap the Au_{13} clusters and thus prevent them from further growth. In the

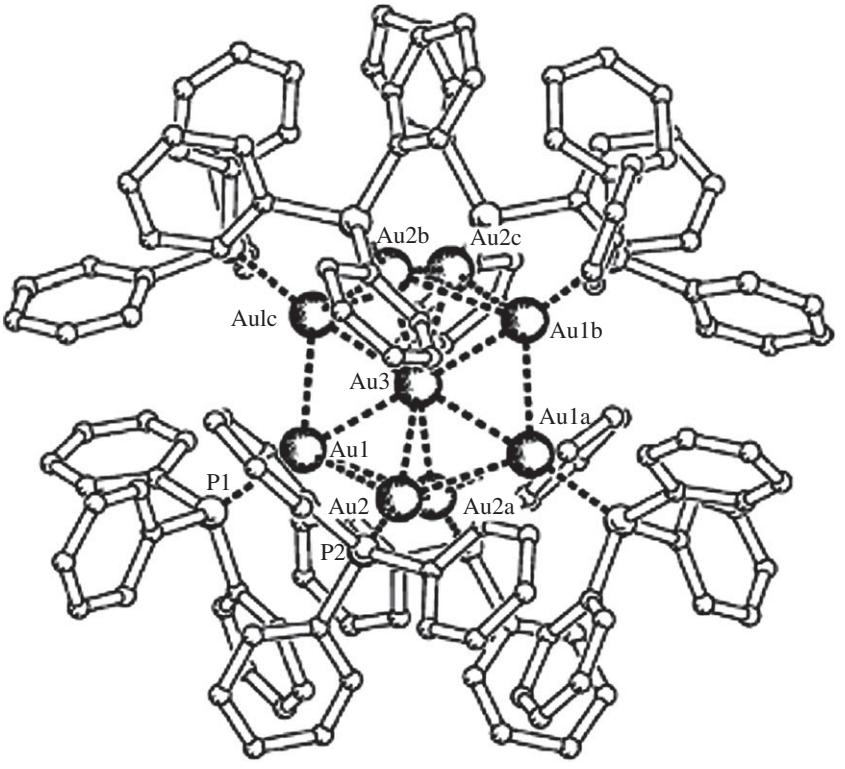

Figure 4. Structure of the $[Au_9(P(C_6H_5)_3]_8]^{3+}$ cluster cation determined by single crystal X-ray measurements. Reproduced with permission from Wen *et al.* (2008). Copyright © Wiley-VCH Verlag GmbH & Co. KGaA.

case of $[Au_{13}(PMe_2Ph)_{10}Cl_2](PF_6)_3$, the cluster was formed by the addition of $Ti(\eta\text{-}C_7H_8)_2$ to a toluene solution of $AuCl(PMe_2Ph)$. Upon redissolution in ethanolic solution and addition of NEt_4Cl, the Au_{13} species crystallized as dark red crystals. Details of this unexpected reaction are still unknown.

There are also several other molecular gold clusters that have been known for many years, which consist of an atom number that does not allow the formation of a closed geometric shell: $Au_8(PPh_3)_7(NO_3)_2$ ('Au_8') (van der Velden *et al.* 1981*b*), $Au_9[P(C_6H_5)_3]_8(NO_3)_3$ ('Au_9') (Wen *et al.* 2008) (figure 4) and $Au_{10}Cl_3(PCy_2Ph)_6NO_3$ ('Au_{10}', Cy = cyclohexyl), just to mention a few. In the case of Au_8 and Au_9, the metal core forms an incomplete icosahedron, and in the case of Au_{10}, the core can be described as a hexagonal ring of six edge- and face-sharing tetrahedral atoms with a central Au atom. The preparation of each single cluster is very specific, and the procedure for the preparation of clusters with a designated size cannot be predicted, which means that the preparation of each cluster material until now has relied mainly on empirical optimization.

Several theoretical attempts, mainly based on large-scale density functional theory calculations, have been performed in recent years to understand and predict structural and compositional features of ligand-protected gold clusters, consisting of an atom number that does not allow the formation of a closed

geometric shell (Häkkinen 2008). Among these is the 'superatom' principle, introduced by Khanna & Jena (1992) for special metal clusters produced in the gas phase, and the 'divide and protect' principle, developed by Häkkinen *et al.* (2006) for an Au_{38} cluster. The superatom principle is based, in analogy to the atomic theory, on the full electron-shell model and was first proposed to explain the stability of certain metal-atom clusters yielding the magic number series 2, 8, 18, 34, 58, etc. by shell closing of the superatom orbitals 1S, 1P, 1D. The divide and protect theory says that gold atoms in thiolate-protected gold clusters are split into two groups: one that forms the metallic core and one that helps to protect the metallic core. These concepts are consistent with the recent ground-breaking experimental studies involving the first crystallization and X-ray structure determination of a thiolate-protected Au_{102} cluster, presented by Jadzinsky *et al.* (2007). The X-ray structure study revealed that pairs of 'thiolate' groups extracted gold atoms from the gold cluster surface layer, thus forming a linear thiolate–gold–thiolate bridge while interacting weakly with the metal surface below, and thus confirmed the theory of the protecting gold–thiolate layer. A detailed analysis of the experimentally determined atomic structure of $Au_{102}(p\text{-MBA})_{44}$ (MBA, mercaptobenzoic acid) combined with the full-density functional treatment of the electronic structure, recently performed by Walter *et al.* (2008), yielded a detailed description of the observed structural motifs and the underlying reasons for the thermodynamic stability of this compound. Along with these findings, the atomic structure of this cluster can be described as an Au_{79} metallic core, displaying approximately D_{5h} symmetry and a protective oligomeric gold–thiolate layer consisting of $Au_{23}(p\text{-MBA})_{44}$ (figure 5).

Thus the gold atoms in the cluster are in two distinct chemical states: the 79 Au atoms of the gold core are in the metallic (charge neutral) state and the 23 Au atoms that belong to the protecting $RS(AuSR)_x$ oligomeric units are oxidized.

The calculated HOMO–LUMO gap of approximately 0.5 eV is significant, and it indicates an atypical electronic stability of the compound. Besides the Au_{102} cluster, Walter *et al.* (2008) also investigated the electronic structures for the following cluster: $Au_{39}(PR_3)_{14}X_6^-$, $Au_{11}(PR_3)_7X_3$ and $Au_{13}(PR_3)_{10}X_2^{3+}$. Based on these investigations, a tool is provided to predict the structures of other stable gold cluster compositions, e.g. $Au_{144}(SR)_{60}$ (Lopez-Acevedo *et al.* 2009).

3. AuNPs as building blocks for nanoelectronics

With modern microelectronics, transistors and other microelectronic devices get smaller and smaller. Along with miniaturization, distances between transistors and related switching elements on a chip get shorter and quantum effects become relevant. Today's nanolithographic fabrication techniques allow scaling down to 50 nm or below (Okazaki & Moers 2005; Li *et al.* 2009). This has already made a great impact on the performance of traditional semiconductor circuits, and it opens up new opportunities utilizing quantum effects. Following the utilization of charging effects, the so-called Coulomb effects, in metallic circuits comprising tunnel junctions with submicron sizes, allow us to handle individual charge carriers. This field has been named single electronics (SE) (Grabert 1991).

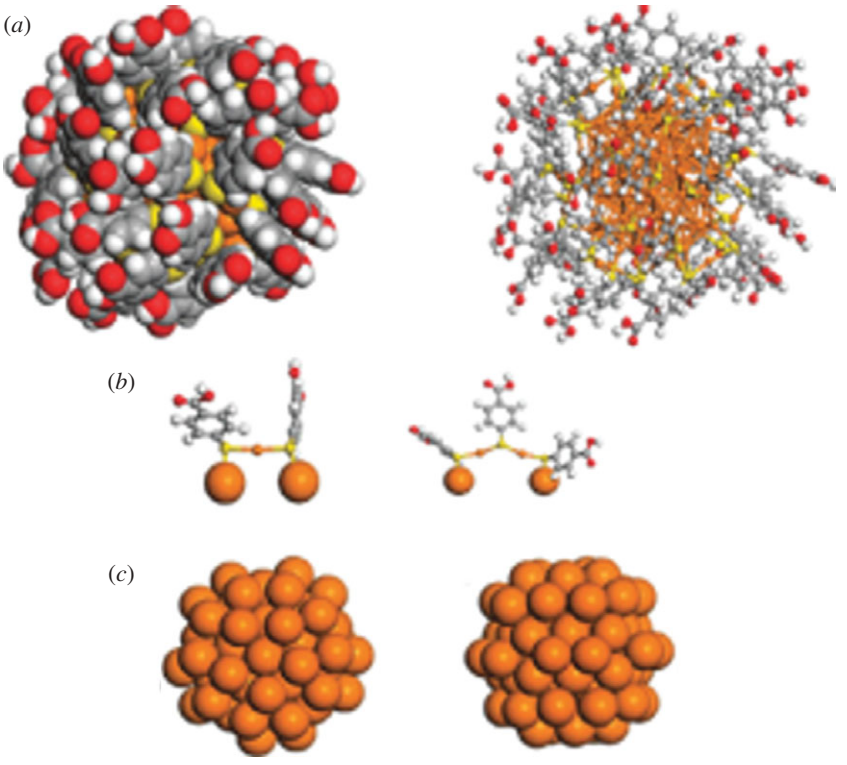

Figure 5. (*a*) Two views of the $Au_{102}(p\text{-MBA})_{44}$ cluster. (*b*) The protecting RSAuSR and $SR(AuSR)_2$ units bound to the core Au atoms (large balls). (*c*) Two views of the Au_{79} decahedral core. Au, brown; S, yellow; C, grey; O, red; H, white. Reproduced with permission from Walter *et al.* (2008). Copyright © 2008, National Academy of Sciences, USA.

SE itself was developed in the late 1980s when intense experimental and theoretical studies on ultra-small metal–insulator–metal sandwich structures (tunnel junctions) and simple systems including these were performed (Likharev 1987, 1988). SE relies on the discreteness of the electric charge, and the tunnelling of electrons in a system of such junctions can be affected by Coulomb interaction of electrons, which can be varied by an externally applied voltage or by injected charges. As the continuous miniaturization in microelectronics reaches its physical limits, new concepts are required to achieve component sizes of tens of nanometres or less, or, ideally, the molecular level. Thus, the idea of utilizing the principle of SE for the development of logic and memory cells, which in principle could lead to the construction of a computer working on single electrons, realizing a 'single-electron logic', has triggered intense research activities related to SET phenomena.

Theoretical and experimental investigations discussed so far have proved that it is possible to observe SET on individual ligand-protected metal nanoparticles (Simon *et al.* 1993*a*,*b*; Schmid *et al.* 2006; Koplin & Simon 2007). Generally, the set-up to probe the tunnelling characteristics of metal nanoparticles involves electrochemical methods, nanometre-separated electrodes (nanogaps) and scanning tunnelling microscopes (STMs). In the following, we

will briefly summarize the basic principles of SET and present selected examples involving STMs and the nanogap set-up with respect to electrical addressing and device formation. Concerning the electrochemical properties, which also reflect Coulomb charging effects, we refer to recent reviews (Laaksonen *et al.* 2008; Zabet-Khosousi & Dhirani 2008), since a detailed description would far exceed the scope of this review. It should just briefly be mentioned that multiple charging becomes feasible in an electrochemical environment (Mertens *et al.* 2009), which could be relevant for multistate logic (Albrecht *et al.* 2007).

(*a*) *The working principle of single-electron devices*

In the following section, we give a brief description of the working principle of SE-based elements. In a macroscopic metallic conductor, electrical current is based on the motion of a huge amount of free electrons through the entire conductor. Despite the discrete nature of the charge carriers, the current flow in a metal is quasi-continuous. In contrast, in an isolated nanoscaled piece of metal (the so-called metal nano-islands), the number of electrons becomes countable. An electrical circuit of such nano-islands should present a number of reservoirs for free metallic electrons, which are separated by poorly permeable tunnelling barriers. In such a configuration, handling of individual charges becomes possible, if the characteristic electric capacitance C of the island is small enough, i.e. the charging energy is large enough to overcome thermal fluctuations. Under these conditions, such a small and defined number of excess electrons on islands change their distribution over the islands in time in a desirable way. This is the concept of single charge storage (SCS) and the respective electronic transport process is called SET.

Experimental observation depends on two principal prerequisites that need to be satisfied.

— The separating insulating barriers should be much higher than the resistance quantum, $R_q = h/e^2 = 25.8\,\mathrm{k\Omega}$.
— The energy associated with charging by one extra, i.e. the charging energy E_C, exceeds the characteristic thermal energy $k_B T$. E_C depends on the charge Q, on the size of the island, and the charge of capacitances of junctions, gates, conductors, etc. in the vicinity of the island. The smaller the island the smaller the capacitance and larger the E_C as well as the temperature, at which single-electron charging can be observed experimentally.

(*b*) *The single-electron box*

The simplest storage device is the single-electron box for injected/ejected electrons, in which the numbers of electrons in a quantum dot (island) are controlled externally (Waser 2005) (figure 6).

Such an element can be implemented into a charge-state logic, which is based on bistable or even multistable configurations, if more than one charge is deposited on the metallic island. In such a configuration, one electron represents one bit, and it can be transferred from one island to the next. Owing to the small number of charge carriers, power consumption of such a device is extremely small, which may be advantageous concerning the minimization of power loss

Figure 6. The tunnelling of a single electron between two metal electrodes through an intermediate island (quantum dot) can be blocked by the electrostatic energy of a single excess electron trapped on the central island. In the case of non-symmetric tunnelling barriers (e.g. tunnelling junction on the left and ideal (infinite resistance) capacitor on the right), this device model describes a 'single-electron box'. Reproduced with permission from Schmid (2004). Copyright © 2004 Wiley-VCH Verlag GmbH & Co. KGaA.

and heat development. However, the unavoidable drawback of SET logic devices is actually the large output impedance, which makes the elements intrinsically slow. Furthermore, such elements are extremely sensitive towards background charges. Thus, the application of SET elements will apparently be restricted to charge sensing and memory elements.

(*c*) *The single-electron transistor*

A switching device, capable of ultra-large-scale integrated circuits, comprises only one Coulomb island with two leads (electrodes) and a capacitively coupled gate electrode attached to it. Such a device may work as a simple on/off switch, and it is often called the single-electron transistor, in which the applied gate voltage U_G serves as a current control.

It has been discussed that such elements may be used in devices with non-volatile memory function as well as in SET/CMOS hybrid circuits, working even at room temperature (Uchida *et al.* 2002). In principle, such transistor elements can be fabricated with different techniques, ranging from silicon-based technology up to chemical SA. However, owing to the minute size, the highest integration rate might be expected from chemically based concepts, where metal or semiconductor nanoparticles assembled at nanocontacts form simple or complex elements with single or multiple SET functions.

(*d*) *SET on individual AuNPs*

As mentioned earlier, set-ups to probe the tunnelling characteristics of metal nanoparticles involve nanometre-separated electrodes (nanogaps) and STMs. STM measurements are based on the principle that, when a sharp metallic tip approaches a non-isolating sample, a tunnelling current can be detected. The tunnelling current depends exponentially on the tip-to-sample distance. This is the basis for imaging the topography of samples. To determine the I–V characteristics, STS investigations can be performed. Thereby, usually, the tip-to-sample distance is fixed and, depending on the tip-to-sample bias, the tunnelling current, differential conductance and so on are measured. The obtained spectroscopic data provide information about local electronic characteristics of the sample, such as density of states (Zabet-Khosousi & Dhirani 2008). One advantage of STM/STS measurements is that the individual cluster can be topographically and spectroscopically analysed in one single experiment, which ensures reliable data.

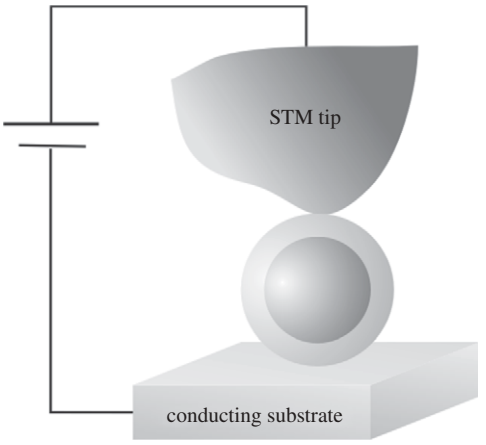

Figure 7. Experimental set-up to image and investigate ligand-protected nanoparticles by STM and STS, respectively.

The experimental set-up to image and investigate ligand-protected nanoparticles by STM and STS, respectively, is depicted in figure 7. The conditions to observe single-electron transitions are $e^2/2C >> k_B T$, where $C = \varepsilon\varepsilon_0 A/d$ is the capacity of the tunnel contact, in which ε is the dielectric constant, ε_0 the electric field constant, A the surface of the electrode and d the distance of the electrodes.

Chi *et al.* (1998) investigated Au_{55} monolayers on various substrates by this method. The monolayers were obtained by a two-step self-assembly (SA) process and a combined Langmuir–Blodgett/SA process. The STS measurements of these monolayers revealed clear evidence of a Coulomb blockade originating from the double barrier at the ligand-stabilized cluster as the central electrode up to room temperature.

By fitting the data obtained experimentally at 90 K, a capacity of 3.9×10^{-19} F for the cluster could be calculated (figure 8). This value is in good agreement with the value of the microscopic capacity determined earlier by temperature-dependent impedance measurements (Schön & Simon 1995*a*).

Low-temperature tunnelling spectroscopic investigations on individual Au_{55} clusters under ultra-high vacuum conditions at 7 K revealed clear Coulomb blockade effects in accordance with the above-mentioned results (Zhang *et al.* 2003). In the Coulomb blockade regime, the conductivity appears to be largely suppressed, but it is not zero, which is attributed to a certain probability of co-tunnelling within the Coulomb gap at 7 K. At this temperature, thermal motion is sufficiently reduced and the molecular structure of the ligand shell becomes partly visible in the STM-resolved topography. The STM image obtained fits fairly well to the proposed space-filling model of the cluster (figure 9).

In figure 9, the two locations at which tunnelling spectra have been recorded are indicated as ‘a’ and ‘b’. The location indicated as ‘a’ is just above a C_6H_5 ring of the PPh_3 ligand, whereas ‘b’ is next to the ring. The resulting tunnelling spectra are depicted in figure 10. The conductivity peaks precisely coincide for both spectra, which shows that the discrete energy levels of the cluster become visible in terms of conductivity oscillations with an average level spacing of 135 meV.

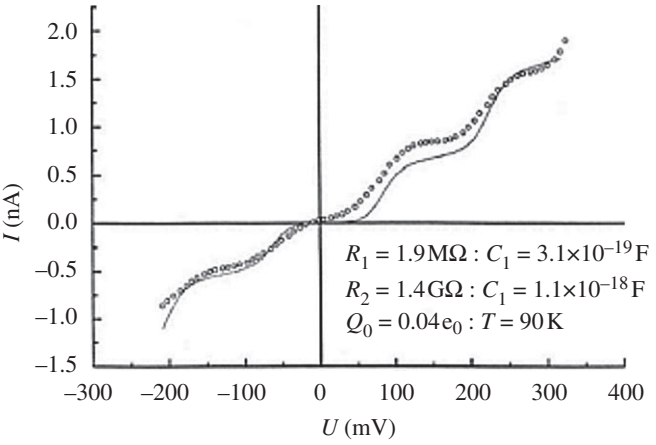

Figure 8. SET on a single ligand-stabilized Au_{55} cluster at 90 K. The junction capacity was calculated to be 3×10^{-19} F by fitting. Continuous line denotes fit; dotted line denotes data. Reproduced with permission from Chi *et al.* (1998). Copyright © Springer Science+Business Media.

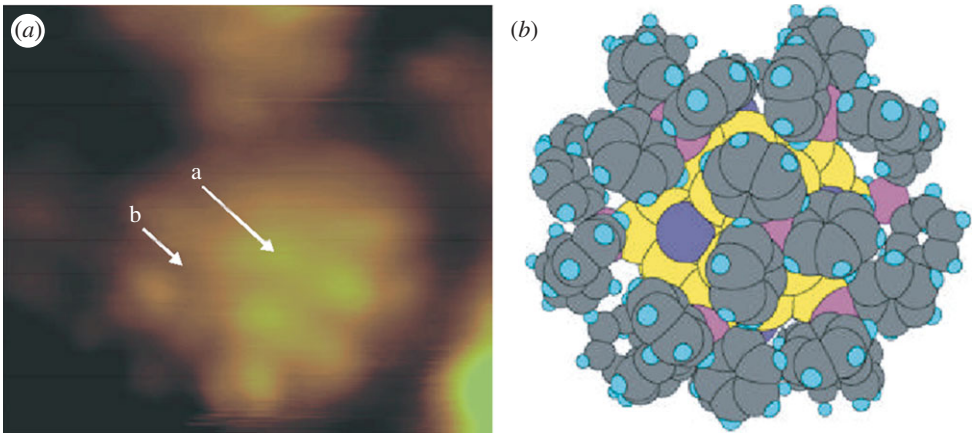

Figure 9. (*a*) STM image of a single $Au_{55}[P(C_6H_5)_3]_{12}Cl_6$ cluster on an Au(111) surface at 7 K, obtained at a bias of 2 V and a current of 100 pA using a Pt–Ir tip. Image size: 3.3×2.9 nm. (*b*) Space filling model of the cluster compound: cuboctahedral core with 55 Au atoms (yellow), 12 $P(C_6H_5)_3$ molecules (with P pink, C grey and H blue) bound to the 12 edges of the cuboctahedron and six Cl atoms (violet) located in the centre of the six square faces of the Au core. Comparison between 'a' and 'b' shows that the STM resolves the C_6H_5 rings. Spectroscopic data were acquired at the two distinct locations marked in (*a*). Reprinted with permission from Zhang *et al.* (2003). Copyright © 2003 American Chemical Society.

With respect to the utilization of these effects by incorporating nanoparticles into single-electron devices, three key aspects have to be taken into account: reliable contact formation of long-term stability, the nanoparticle size and the nature of the ligand shell. The nature of the ligand shell influences the current

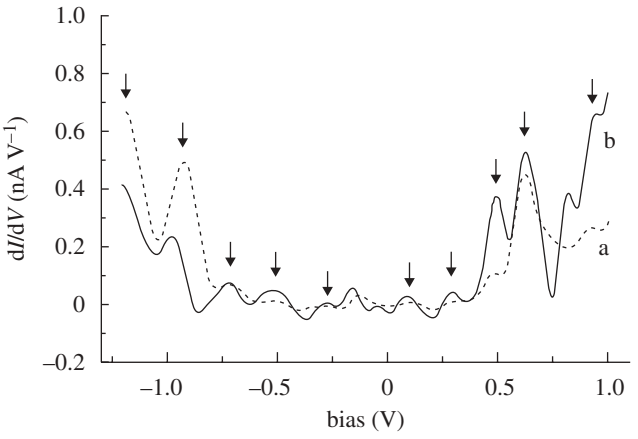

Figure 10. Tunnelling spectra acquired at the two distinct locations marked in figure 9*a*. The dashed curve was taken right above the C_6H_5 ring and the solid ones next to the ring. The bias refers to the substrate potential. The arrows indicate conductivity peaks, which precisely coincide for both spectra. Reprinted with permission from Zhang *et al.* (2003). Copyright © 2003 American Chemical Society.

flow through the substrate/ligand/nanoparticle structures, displaying a double-barrier tunnel junction, as the 'transparency' of the ligand shell is dependent on the 'thickness', the composition and possible charge states. Thus, the current flow through such a device is sensitive to any charges and impurities that reside on the nanoparticles or in the ligand shell.

One example in this context is the recently published work of Xu & Chen (2009) on STM/STS investigations of various hexanethiolate-protected (3.2–6.3 and 11.8 nm) AuNPs concerning the change in the tunnelling characteristics upon exposure of the nanoparticle/SAM/gold structure to organic vapours. The organic vapour molecules penetrate the nanoparticle/SAM interface and thus modify the tunnel junction. For the particles with a diameter of around 6 nm, these investigations revealed a drastic enlargement of the Coulomb gap in the I–V characteristics with increasing vapour concentration and decreasing vapour relative polarity.

This sensitivity of the ligand shell towards 'impurities' opens up the possibility of chemically controlling the 'transparency' of the ligand shell with respect to manipulating the SET current. This fact leads to the concept of chemical gating.

One example in this context was presented by Gittins *et al.* (2000), who reported on STM/STS investigations of ligand-stabilized AuNPs (6 nm), whereby the ligand shell consists of viologene derivatives. Viologene is a redox active molecule. It was found that, by incorporating electrons into the redox-active viologene group under electrochemical control, the transparency of the insulating barriers (the ligand shell) could be modified, i.e. it was found that reduction of V^{2+} to the radical V^{+} led to a significant decrease in the barrier height, whereas further reduction to V^{0} resulted in a very large increase in the barrier height. These results show that switching of the SET current through a ligand-stabilized nanoparticle can be induced by electron injection into a specific redox group within the barriers of the tunnel junction.

Similar to the above-mentioned work, Brousseau *et al.* (1998) provided an electrochemical gating approach to control the charge transport through the tunnel junction substrate/ligand/nanoparticle by utilizing pH-dependent changes of galvinol, which upon increasing the pH is converted to galvinoxide anion, and thus making the ligand shell negatively charged. Additionally, Albrecht *et al.* (2007) reported on the fact that dielectric saturation effects in the immediate surroundings of the charged nanoparticles also influence the observed tunnelling characteristics.

Although the above-mentioned examples demonstrate that, in principle, the STM set-up can be used to electrically address and control the I–V characteristics of individual nanoparticles by electrochemical means, this set-up is limited with respect to device fabrications. The alternative approach is to utilize nanometre-spaced electrodes, the so-called nanogaps. In such a set-up, control of the tunnelling current can be achieved by introducing a third electrode as a gate and by applying a gate voltage. Nevertheless, such a set-up is accompanied by a huge number of technical difficulties. One challenge is to fabricate such small structures that allow contact between individual metal nanoparticles with sizes of a few nanometres. Furthermore, owing to the fabrication process including the nanogap formation itself and the immobilization of individual metal nanoparticles into the gap, the device-to-device variations are large and require statistical analysis of a large number of samples. Moreover, details on the contact between the electrode and the nanoparticle are still less characterized. However, nowadays, electron-beam lithographic techniques allow already nanogap configurations with gap separations of approximately 10–100 nm. Furthermore, gaps of less than 10 nm can be created by, for example, mechanical breaking or electromigration (Zabet-Khosousi & Dhirani 2008). This means, in principle, that addressing of individual AuNPs is achievable, although, nevertheless, the number and the orientation/topologies of AuNPs in such a nanogap are still hard to control.

One early example that demonstrates this principle for electrical addressing of individual ligand-stabilized nanoparticles immobilized within a nanogap was given by Klein *et al.* (1996). In a sophisticated approach, they combined optical lithography and angle evaporation techniques to produce narrow gaps of a few nanometres. The immobilization of AuNPs (5.8 nm) between the gold leads in the nanogap was achieved by chemically controlled assembly from solution upon utilizing the bifunctional linker hexane-1,6-dithiol, which forms stable thiolate/gold bonds. The resulting device revealed weak current steps in the $I(V)$ characteristic at 77 K. By fitting to the classical Coulomb blockade models, a junction capacity of 2.1×10^{-18} F could be calculated. With respect to the production of an SET transistor in a further development, a gate electrode was introduced to externally control the current flow. The basic working principle of such a device was proved by immobilization of Au and CdSe nanoparticles (Klein *et al.* 1997). Nevertheless, the difficulty in the fabrication process becomes clear upon looking at the success rate. For example, for leads with less than 20 nm spacing and in the case of AuNPs, three of 50 devices showed the characteristic Coulomb blockade. However, in contrast to STM-based set-ups, these devices turned out to be relatively stable under ambient conditions for a few weeks.

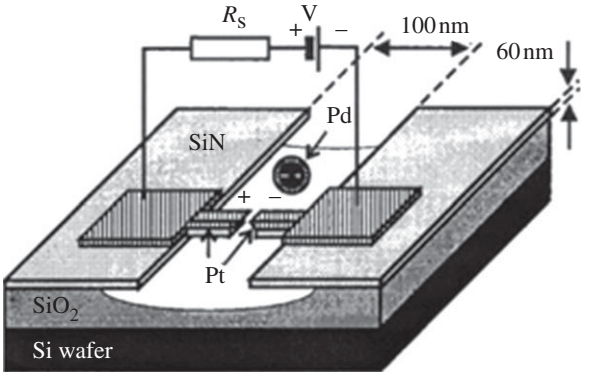

Figure 11. Schematic of the set-up for single particle measurements. Pt denotes two free-standing Pt electrodes (dashed region). A ligand-stabilized Pd cluster is polarized by the applied voltage and attracted to the gap between the Pt electrodes (ET). Reprinted with permission from Bezryadin *et al.* (1997). Copyright © 1997 American Institute of Physics.

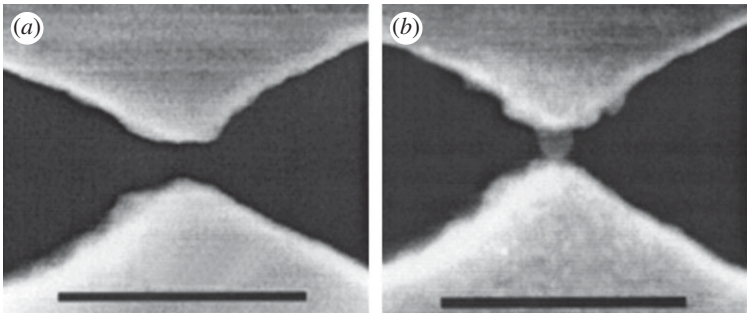

Figure 12. (*a*) Pt electrodes (white) separated by an approximately 14 nm gap. (*b*) After ET, the same electrodes are bridged by a single, approximately 17 nm Pd particle. Reprinted with permission from Bezryadin *et al.* (1997). Copyright © 1997 American Institute of Physics. Scale bar, (*a*,*b*) 100 nm.

Schmid and Dekker used electrostatic trapping (ET) for the controlled deposition of individual palladium nanoparticles in a 4 nm nanogap (figure 11) (Bezryadin *et al.* 1997). ET is based on the attraction of a polarized metal nanoparticle to the strongest point in an electric field, which is applied between two electrodes.

Nanogap sizes of 4 nm were achieved as follows. In the first step electrodes were produced by thermal growth on silicon. In the second step, a 60 nm SiN film was deposited on top of these structures and in the following step a 100 nm slit in the SiN film with 20 nm spacing was opened by electron beam lithography utilizing a poly(methylmethacrylate) (PMMA) shadow mask technique. Etching of these obtained structures with hydrogen fluoride led to free-standing SiN 'fingers' and, finally, sputtering with Pt resulted in gap sizes of around 4 nm (figure 12).

The characteristic $I(V)$ curves obtained by this set-up are shown in figure 13. The most pronounced feature is the Coulomb blockade characteristic at a voltage of approximately 55 mV and a temperature of 4.2 K, which disappears at 295 K.

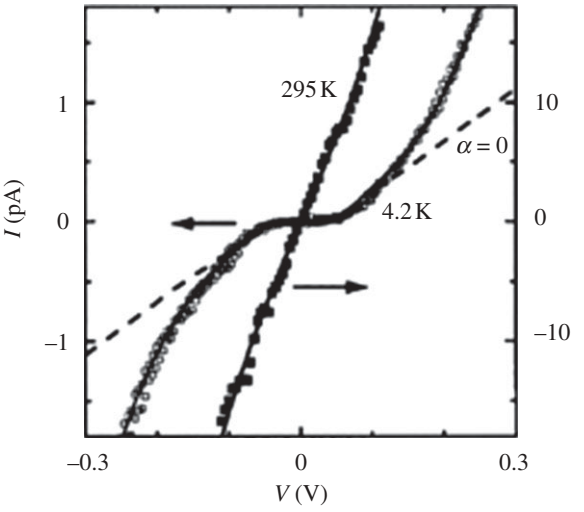

Figure 13. Current–voltage curves measured at 4.2 K (open squares) and at 295 K (solid squares). The solid curves denote fits of theoretical calculations according to the model proposed by Korotkov & Nazarov (1991). Fitting parameters for these curves are $V_c = 55\,\mathrm{mV}$, $R_0 = 1.1 \times 1011\,\Omega$, $q_0 = 0.15e$ (offset charge) and $a = Ec/h = 0.5$. The dashed curve ($\alpha = 0$) represents the conventional model that assumes a voltage-independent tunnel barrier. Reprinted with permission from Bezryadin *et al.* (1997). Copyright © 1997 American Institute of Physics.

Furthermore, the $I(V)$ curve above the gap increases exponentially instead of linearly. The latter fact was explained by the suppression of the effective tunnel barrier by the applied voltage.

The above-mentioned early examples demonstrate that, in principle, the nanogap set-up can be used for the fabrication of stable SET transistors based on a single nanoparticle, but the effort required to create such small nanogaps that satisfy the requirements for small metal nanoparticles is huge, especially for devices working at ambient temperature, as this requires nanoparticles of sizes below 2 nm.

In this context, we proposed a concept that would display one first step in the line of device fabrication and would circumvent at least some of the above-mentioned difficulties: a cross-bar system consisting of conducting wires of 2.5 nm in diameter, arranging, for example, Au_{55} clusters strictly one dimensionally and having a switch between each cross-point. This would allow us to electrically address each individual Au_{55} cluster. The intended arrangement is depicted in figure 14.

Along with the fabrication of such a structure, a multilayer system of epitaxially grown alternating GaAs and AlAs layers has already been developed (Schmid *et al.* 2008). This multilayer system was partly oxidized by H_2O_2, followed by an etching process with citric acid and repeated oxidation. The successful generation of the 20 nm Al_2O_3 bar system has been demonstrated by atomic force microscope (AFM) and scanning electron microscope (SEM) measurements. Shadow mask evaporation of gold finally gives conductive bars that were decorated with Au_{55} clusters via the bifunctional linker molecule 1,4-benzenedithiol. The presence of the clusters has been proved by electrical

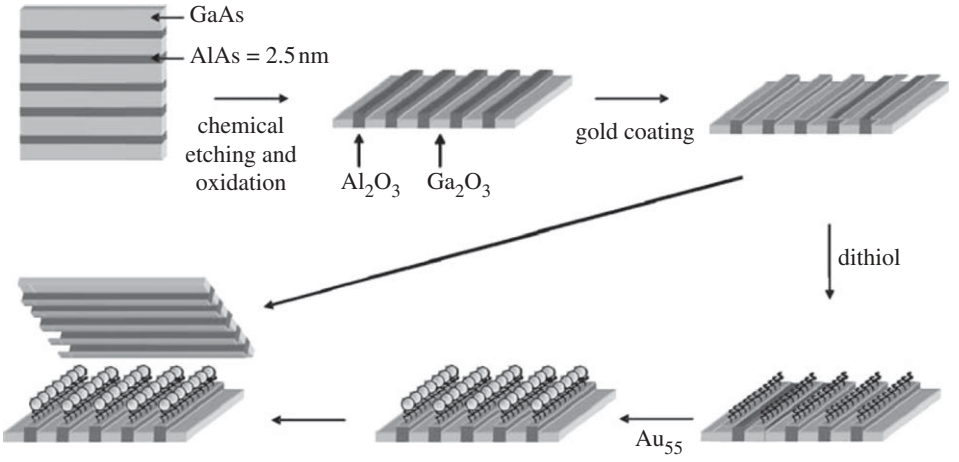

Figure 14. Sketch of intended construction of a cross-bar system with single quantum dots between each cross-point. Reproduced with permission from Schmid (2008). Copyright © The Royal Society of Chemistry.

measurements before and after the decoration. The cluster-protected bars showed a drastically increased resistivity. Furthermore, it has already been demonstrated that 2.5 nm Al_2O_3 bars can also be generated by the same technique. Although the deposition of gold clusters on the 2.5 nm bars has not yet been performed, the above-mentioned results are very promising with respect to successful further development.

(*e*) *Strategies for nanoparticle assembly*

The results of early investigations related to the formation of SET transistors built up from individual nanoparticles are promising, but with respect to the formation of devices such as nanoswitches or SET transistors working under ambient conditions, the effort for the fabrication of such devices is huge. Approaches that can overcome at least the lithographic limitations use assemblies of nanoparticles. However, a further key aspect comes into focus: in order to fabricate reliable and reproducible devices, the assembly of nanoparticles, as well as the immobilization progress, needs to be highly controllable. In this context, many protocols for the three-, two- and one-dimensional organization of nanoparticle arrangements have already been reported (Murray *et al.* 1993, 1995; Schön & Simon 1995*b*; Alivisatos 1996; Whetten *et al.* 1996; Collier *et al.* 1997, 1998; Kieley *et al.* 1998; Simon *et al.* 1998; Talets *et al.* 1999; Sun *et al.* 2000; Torma *et al.* 2003). Three-dimensional arrangements have been reported intensively, since the first investigations of SET effects in assemblies refer to pellets (Houbertz *et al.* 1994; Simon 1998) and networks (Schmid & Simon 2005). Generally, three-dimensional arrangements are principally based on the utilization of bifunctional linker molecules interconnecting the nanoparticles. Approaches towards two-dimensional arrangements mainly refer to the basic principles presented by Janes *et al.* (1995), whereby a strictly two-dimensional arrangement is achieved in a two-step procedure involving the deposition of nanoparticles from a colloidal solution in the first step, followed by an addition

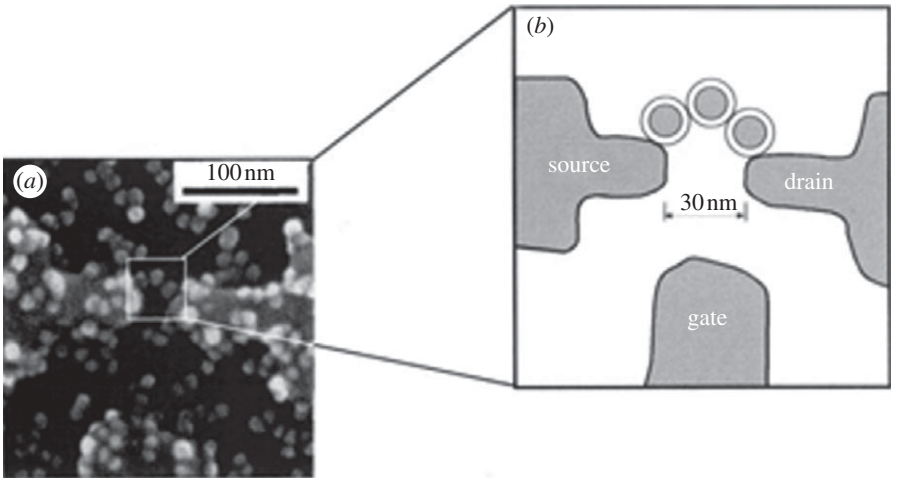

Figure 15. SET transistor based on SA of AuNPs on electrodes fabricated by electron beam lithography. Reprinted with permission from Sato *et al.* (1997). Copyright © 1997 American Institute of Physics. Scale bar, (*a*) 100 nm; (*b*) 30 nm.

of bifunctional molecules that are capable of interconnecting the nanoparticles within the monolayer, as in the three-dimensional case. In the following, we will focus on recently presented promising new ideas for the one- and two-dimensional organization with respect to applications in nanoelectronics.

(i) *One-dimensional assemblies*

Sato *et al.* (1997) first presented a single-electron transistor using an ordered one-dimensional array consisting of two to four AuNPs. They bridged a 30 nm gap formed by electron beam lithography with AuNPs of sizes around 10 nm. The method to achieve this was described as follows. In the first step, citrate-stabilized AuNPs are immobilized on previously aminosilanized gap structures to form a submonolayer caused by binding of the amino group to the gold surface. In the second step, this submonolayer is treated with 1,6-hexanedithiol that replaces the citrate ligand on the AuNP surfaces and leads to thiol-terminated AuNPs. In the third step, further immobilization of citrate-stabilized gold nanoparticles leads to the formation of nanoparticle chains. The chains consist mostly of two to four nanoparticles (figure 15). The bifunctional dithiol linker acts thereby as a defined spacer between the nanoparticles and the particle–electrode connection and provides the tunnel barriers. From device to device, the number of bridging nanoparticles and the location of these chains varied, but, nevertheless, the observed electrical conduction through these devices showed clear Coulomb staircases and periodic conductance oscillations in dependence of the gate voltage, proving that the desired function of the single-electron transistor had been achieved.

Since this proof of concept, many attempts to achieve one-dimensional arrays immobilized within nanogaps have been performed. For example, Lee *et al.* (2005) selectively assembled 10 nm thiol-modified single-stranded DNA nanoparticles

into nanogaps utilizing the DNA hybridization scheme; Bates *et al.* (2006) used Mg^{2+}-mediated RNA–RNA loop–receptor interaction; Weiss *et al.* (2006) reported on the lithographic contacting of previously SA 50 nm nanoparticles; and Coskun *et al.* (2008) applied pre-structured substrate surfaces to achieve strictly one-dimensional arrangements of 13 and 50 nm sized AuNPs.

Although all these attempts, in principle, prove the concept of utilizing one-dimensional assemblies in SE, they all worked with larger particles and Coulomb charging effects were observed only in the low temperature regime. With respect to potential devices working at room temperature or at least at elevated temperatures, smaller clusters have to be considered for reasons mentioned before.

One example in this context is the formation of one-dimensional cluster chains consisting of $Au_{55}(PPh_3)_{12}Cl_6$ by ET, presented by Schmid *et al.* (2001). $Au_{55}(PPh_3)_{12}Cl_6$ clusters were trapped in a three-tungsten electrode configuration on an SiO_2 surface with a 30 nm gap leading to a quasi one-dimensional arrangement (figure 16*a*,*b*; Schmid *et al.* 2001). Current–voltage measurements of these quantum dot wires at room temperature showed equivalent Coulomb blockades in the region between −0.5 and 0.5 V (figure 16*c*).

Although this method displays a proof of concept, this procedure only leads to quasi-one-dimensional structures and the process of chain formation is poorly controllable, and the assembly and electrical addressing of strictly one-dimensional assemblies of small AuNPs (less than 2 nm) still remain a great challenge. In the following, we will concentrate on approaches concerning a highly controllable formation of strictly one-dimensional cluster arrangements.

Liu *et al.* (2002) utilized chemical modification of an alkyl-terminated SA monolayer. The terminal CH_3 groups were converted into COOH functions by a metallized AFM tip, inducing electric pulses. The COOH groups were further functionalized by SH groups that provide strongly binding anchor groups for the chemically induced immobilization of Au_{55} clusters by substitution of the PPh_3 molecules (figure 17). As an example of the success of this concept, an AFM image of two one-dimensional cluster rows, intentionally interrupted to deposit individual clusters, is illustrated in figure 18. In principle, depending on the software of the AFM, any kind of pattern can be drawn using this technique.

Further attempts use DNA as a template for a strictly and highly controllable one-dimensional assembly of AuNPs. Utilizing DNA as a template is attractive owing to the fact that the extraordinary self-recognition properties, and the possibility of directing the sequence by modern synthetic methods enables the template to be programmed to a high degree. This concept has already been applied in many approaches ranging from electrostatic interactions to full metallization (Alivisatos *et al.* 1996; Loweth *et al.* 1999*a*,*b*; Niemeyer 2001*a*; Xiao *et al.* 2002; Warner & Hutchison 2003; Le *et al.* 2004; Li *et al.* 2004; Woehrle *et al.* 2004; Braun *et al.* 2005; Deng *et al.* 2005*a*,*b*; Niemeyer & Simon 2005; Noyong *et al.* 2007*a*; Fischler *et al.* 2007, 2009).

Very recently, we developed a procedure that exploits the Cu(I)-catalysed Huisgen cycloaddition (‘click’ reaction) between azide and alkyne groups for the immobilization of small metal nanoparticles along artificial DNA strands (Fischler *et al.* 2008). Artificial DNA duplexes modified with alkyne functionalized thymine and cytosine derivatives were synthesized by PCR (Gierlich *et al.* 2007; Rozkiewicz *et al.* 2007). Binding to the DNA was achieved by ‘clicking’ azide-terminated Au nanoparticles of diameters between 1 and 4 nm to the DNA

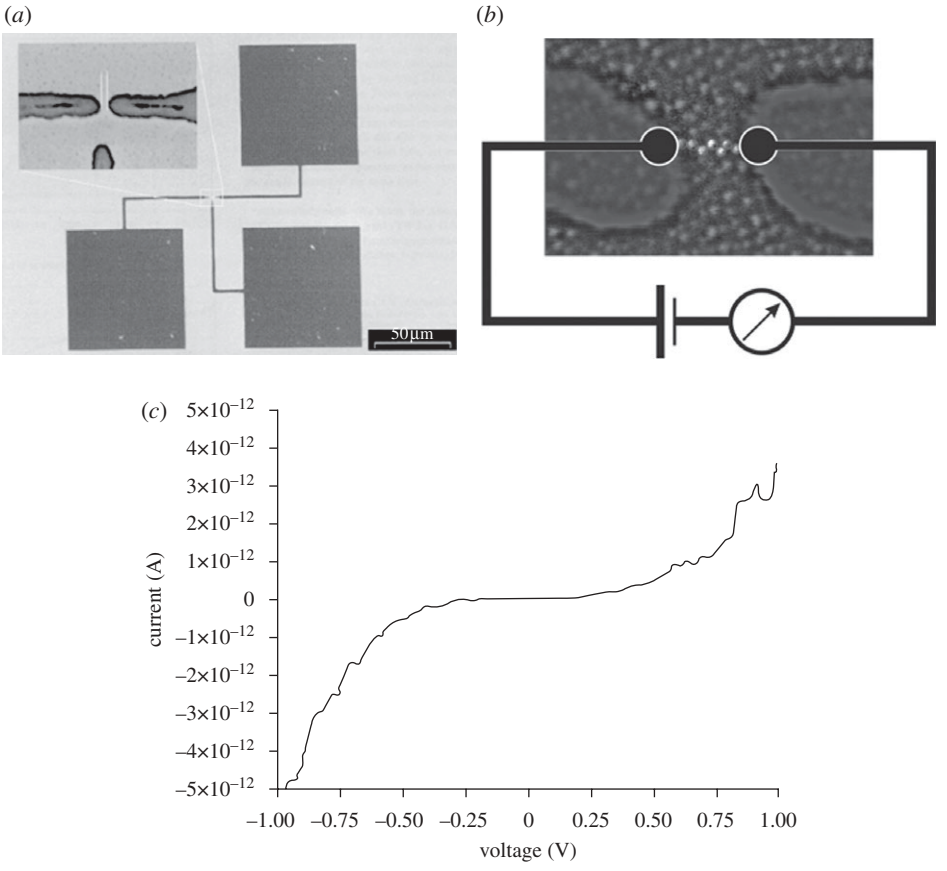

Figure 16. (*a*) SEM image of a three-electrode configuration with source, drain and gate electrodes. The inset shows in magnification the gap in the tungsten electrodes. (*b*) High-resolution SEM of Au_{55} clusters forming a quasi one-dimensional chain. (*c*) $I(V)$ characteristic of the device. Reprinted with permission from Schmid *et al.* (2001). Copyright © 2001 American Chemical Society. Scale bar, (*a*) 50 µm; inset 20.4 nm.

duplexes. Detailed TEM and AFM (figure 19*a*,*b*) studies proved that the one-dimensional nanoparticle arrays obtained consist of uniform nanoparticles with regular particle distance, which is presumably caused by the space requirement of the ligand shell surrounding the particles (figure 19*c*).

Although electrical characterization of these structures has not yet been successful, this approach is very promising with respect to highly controllable one-dimensional assemblies.

In additional investigations, we could demonstrate that the formation of such one-dimensional arrays is restricted to the utilization of preformed nanoparticles. It could be shown that controlled reduction of Ag^+ ions in solution, localized at aldehyde groups of artificial DNA duplexes carrying aldehydes instead of alkynes, is possible (Wirges *et al.* 2008). The redox reaction between the aldehyde groups and the Ag^+ ions resulted in the formation of silver seeds assembled along the

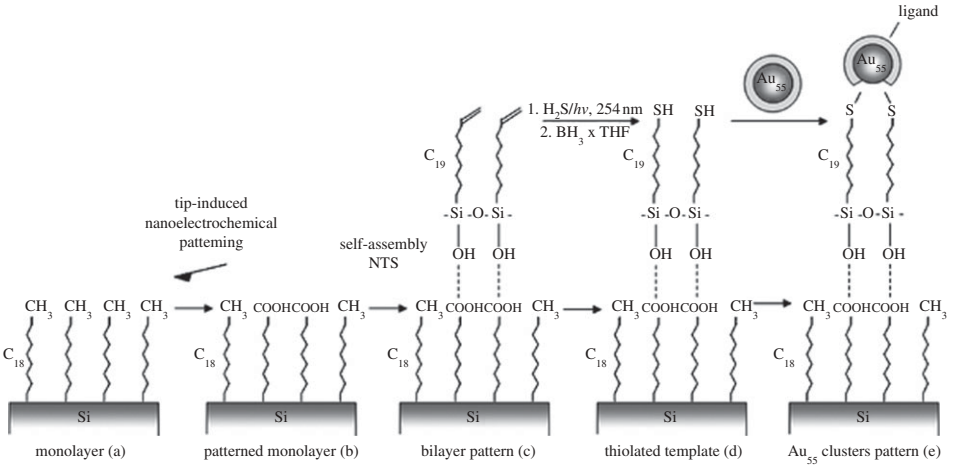

Figure 17. Scheme for the AFM-supported generation of thiol-functionalized monolayer that is capable of binding Au_{55} clusters upon thiolate/gold bond formation. Reproduced with permission from Schmid (2008). Copyright © The Royal Society of Chemistry.

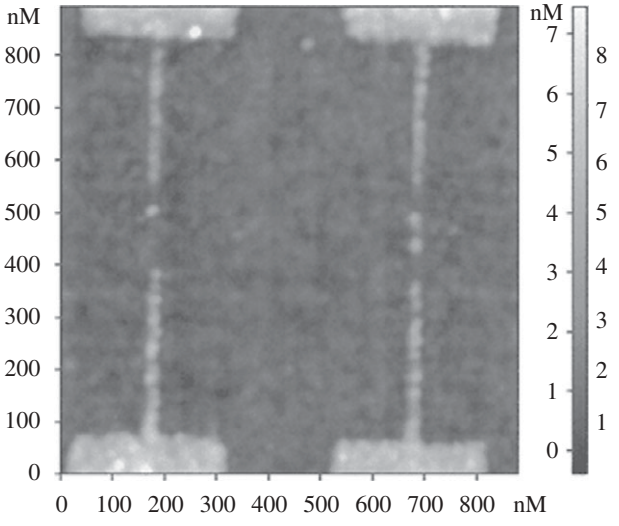

Figure 18. AFM image of strictly one-dimensionally ordered $Au_{55}(PPh_3)_{12-x}Cl_6$ clusters. The one-dimensional wires are intentionally interrupted to deposit one (left) and two (right) individual clusters. Reprinted with permission from Liu *et al.* (2002). Copyright © 2002 American Chemical Society.

DNA strands and one aldehyde group reduces two silver ions resulting in the formation of a Ag_2 cluster, whereas a dialdehyde group forms Ag_4 clusters. This cluster formation was studied in detail by UV–Vis and HR-STEM measurements.

UV–Vis investigations of the cluster formation process comparing monoaldehyde- and dialdehyde-functionalized DNA duplexes, as depicted in figure 20, revealed that the formation of larger clusters is fourfold more efficient along the dialdehyde strands.

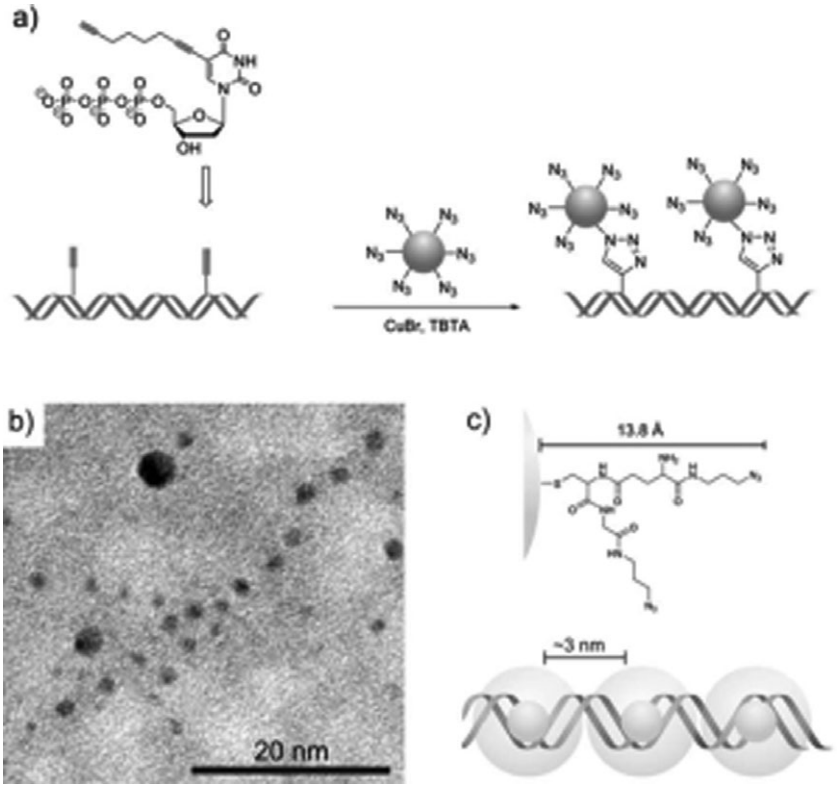

Figure 19. (*a*) Scheme of the incorporation of artificial DNA bases into the DNA strand by PCR, followed by attachment of azide-terminated nanoparticles to the strand via a Cu(I)-catalysed click reaction. (*b*) TEM micrograph of the particles aligned in regular distance on the template. (*c*) The interparticle distance is determined by the space requirement of the nanoparticles' ligand shell, i.e. approximately 1.4 nm for the glutathione bisazide in fully extended conformation. Reproduced with permission from Fischler *et al.* (2008). Copyright © The Royal Society of Chemistry. Scale bar, (*b*) 20 nm; (*c*) approximately 3 nm.

STEM analysis of the monoaldehyde-modified DNA (figure 21*c*) showed the presence of large amounts of small Ag particles formed after treatment with Ag^+ ions (1.2 ± 0.5 nm). Chain-like arrangements of larger silver nanoparticles were also detected, but they were rare and the particle distribution along the chains was rather irregular. The treatment of dialdehyde-modified DNA with Ag^+ ions yielded more chain-like formations (figure 21*d*). A rough estimation of the number of Ag atoms from TEM images indicates that the reduced silver is apparently in excess to the amount of DNA-bound aldehyde groups. Thus, it can be assumed that the initially formed silver nuclei (Ag_4) grow by an auto-catalytic reduction process. The obtained structure could be further metallized in subsequent metal development step by treatment with Tollen's solution, leading to full metallized DNA strands.

Although these concepts were originally developed with the aim of producing conducting nanowires upon metallization of the obtained DNA–nanoparticle assemblies, these approaches bear a promising idea with respect to the formation

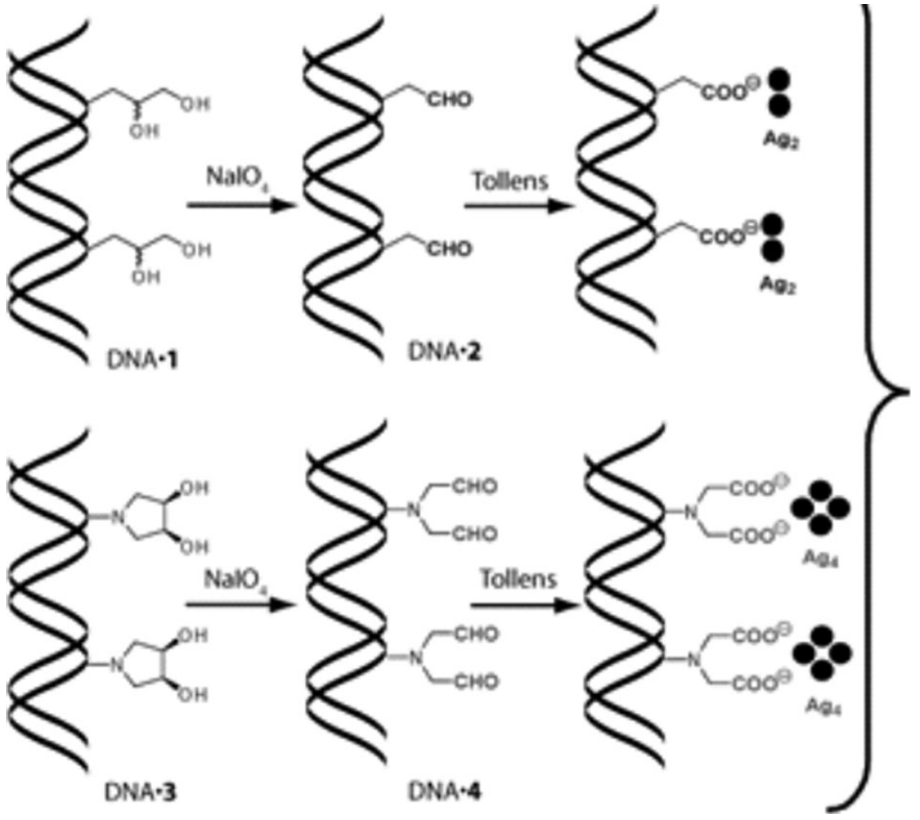

Figure 20. Preparation of monoaldehyde- and dialdehyde-functionalized DNA. Reproduced with permission from Wirges *et al.* (2008). Copyright © 2008 Wiley-VCH Verlag GmbH&Co. KGaA.

of highly controllable electrical addressing of strictly one-dimensional arrays comprising small metal nanoparticles. Preparing DNA templates that comprise both aldehyde and alkyne groups would allow one-dimensional gold cluster formation and formation of conducting to be combined, thus leading to an orthogonal approach for electrical addressing of one-dimensional assemblies.

Contact between nanoparticles or nanoparticle assemblies could be performed by a technique developed in our group for the precise *in situ* addressing of low-dimensional nanostructures involving a nanomanipulator system incorporated in the chamber of an SEM (Noyong *et al.* 2007*b*). Along with this, we recently published investigations on one-dimensional arrays of 44 nm AuNPs applying the nanomanipulator set-up (Blech *et al.* 2008). The nanomanipulators consist of metallized tips that can be individually addressed under simultaneous observation in the SEM (figure 22). The investigated one-dimensional arrays were prepared as follows. In the first step, PMMA-coated Si wafers were structured by extreme-ultraviolet interference lithography. Following this, the formed grooves were filled with the AuNPs by dip coating the substrates into a nanoparticle suspension. Figure 23 displays the corresponding SEM pictures of the contacting process.

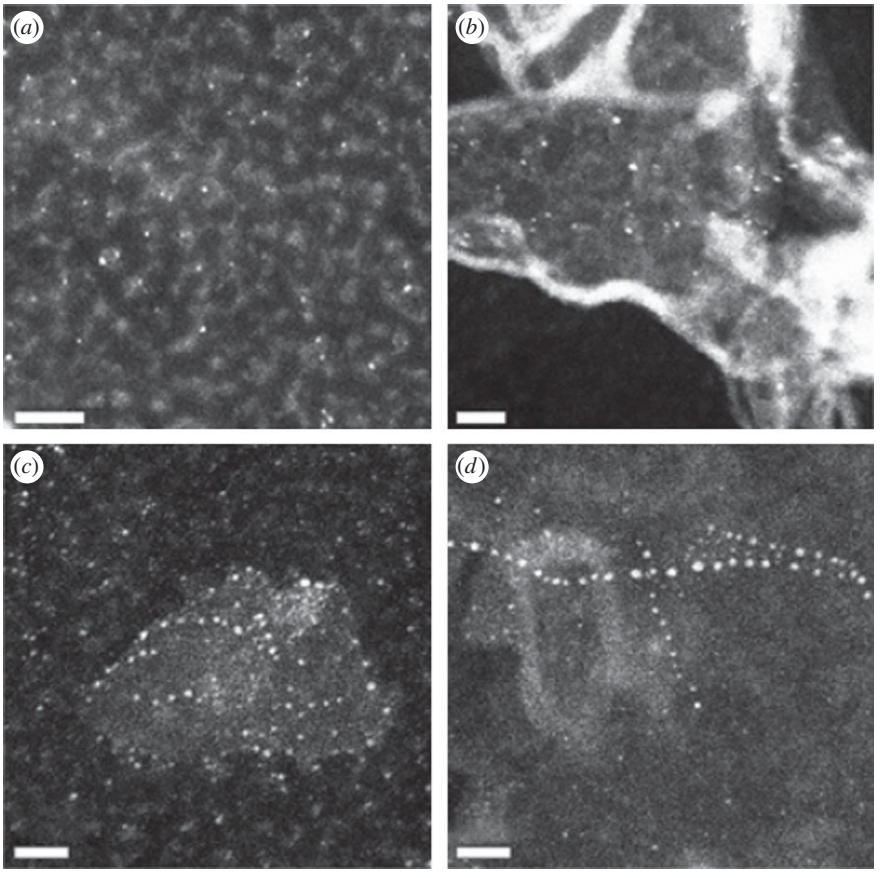

Figure 21. HR-STEM micrographs. (*a*) Tollen's solution without DNA, (*b*) Tollen's solution incubated with unmodified DNA, (*c*) Tollen's solution incubated with 900DNA•2 and (*d*) Tollen's solution incubated with 900DNA•4, for 20 min, respectively. Reproduced with permission from Wirges *et al.* (2008). Copyright © 2008 Wiley-VCH Verlag GmbH&Co. KGaA. Scale bar, (*a–d*) 25 nm.

In order to estimate the influence of the ligand shell on the conduction process, these structures were treated with ozone to produce ligand-free nanoparticles. From the $I–V$ characteristics (figure 23) measured by this set-up, the resistance of an individual particle before and after the ozone treatment could be calculated. The removal of the insulating ligand shell by ozone cleaning resulted in higher conductivity and lower resistance per particle. The results are in good agreement with the data obtained by the previously mentioned, lithographically fabricated structures (Cui *et al.* 2004; Weiss *et al.* 2006) and therefore indicate that this measurement set-up can be used for the routine addressing of structures in the sub-10 nm range.

(ii) *Two-dimensional assemblies*

As mentioned before, two-dimensional assembly strategies are mainly based on the method reported by Janes *et al.* (1995). Similar to this approach, Liao *et al.* (2006) presented a procedure that exploits microcontact

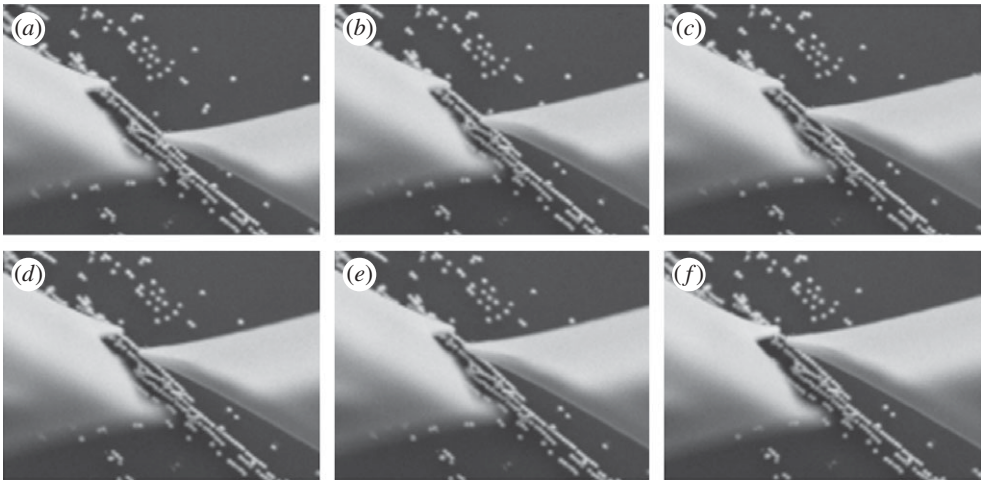

Figure 22. (*a–f*) Corresponding SEM pictures of the electrical transport measurements along decreasing tip-to-tip distance.

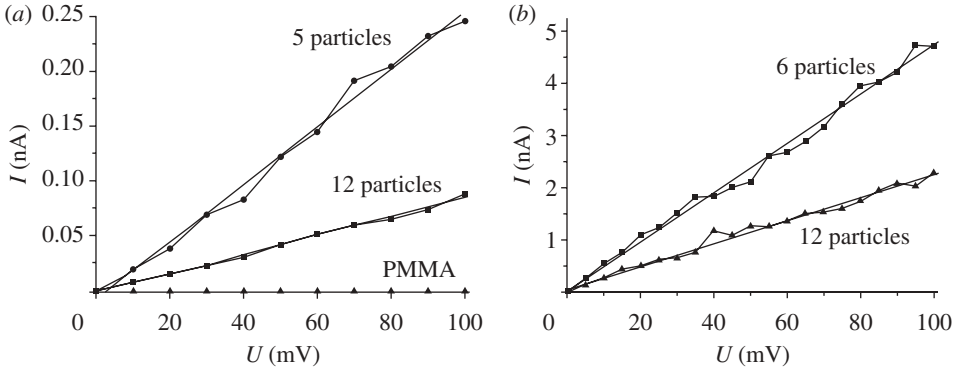

Figure 23. (*a*) *I–V* characteristics of as-prepared AuNP chains with different numbers of particles and a reference measurement on the PMMA surface. (*b*) *I–V* characteristics of O_3-cleaned samples. Reprinted with permission from Blech *et al.* (2008). Copyright © American Scientific Publishers, www.aspbs.com.

printing for the formation of stable two-dimensional arrangements of 10 nm octanethiol-stabilized AuNPs. *In situ* ligand exchange was performed by the addition of a bifunctional OPE (dithiolated oligo(phenylene ethynylene)) in order to interconnect the nanoparticles within the two-dimensional arrangement. The electrical characteristics of the obtained structures were determined by depositing contact pads on top of the monolayers, whereby a TEM grid acts as a shadow mask (figure 24*a*). The electrical characterizations were performed at ambient temperature and revealed a linear characteristic.

In order to compare the resistances at different stages of the exchange experiment, sheet resistances were calculated. For the first step in which the particles are stabilized by octanethiol molecules and interlinked owing

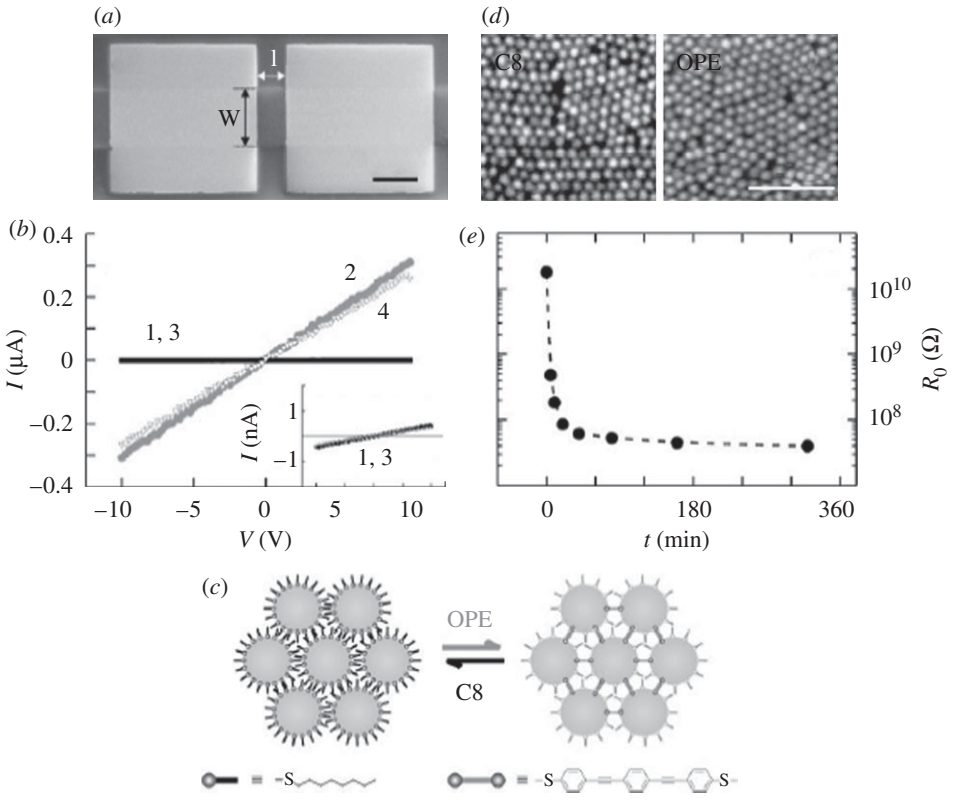

Figure 24. (*a*) Electron microscope image of the investigated device, (*b*) $I(V)$ characteristics of the device at different stages in the exchange experiments, (*c*) scheme of the exchange reaction in the monolayer of the nanoparticles, (*d*) electron microscopy pictures of the nanoparticle array before and after molecular exchange and (*e*) resistance versus immersion time in the OPE measurement during the exchange reaction. Reproduced with permission from Liao *et al.* (2006). Copyright © 2006 Wiley-VCH Verlag GmbH & Co. KGaA. Scale bar, (*a*) 20 μm; (*d*) 100 nm.

to van der Waals interaction between penetrating alkane chains (figure 24*b*, curve 1), a sheet resistance of $4.4 \times 10^{10}\,\Omega$ was calculated. After ligand exchange versus OPE, the sheet resistance was decreased by more than two orders of magnitude ($R_s = 6.3 \times 10^{10}\,\Omega$; figure 24*b*, curve 2). Most interestingly, the electrical transport measurements revealed that the ligand exchange and the process of interlinking by OPE are reversible (figure 24*b*, curves 3 and 4). Thus, this example represents an interesting approach towards chemically triggered switching.

A similar approach was recently reported by van der Molen *et al.* (2009). Two-dimensional lattices of 10 nm octanethiolate-protected AuNPs were produced in the same manner as described earlier, followed by a ligand exchange reaction to replace the octanethiol ligand versus rigid bifunctional dithiolated photochromic diarylethene molecules, thus leading to interconnection of the nanoparticles within the array (figure 25). For the electrical characterization of the arrays, two gold electrodes were evaporated on each array (figure 25*c*).

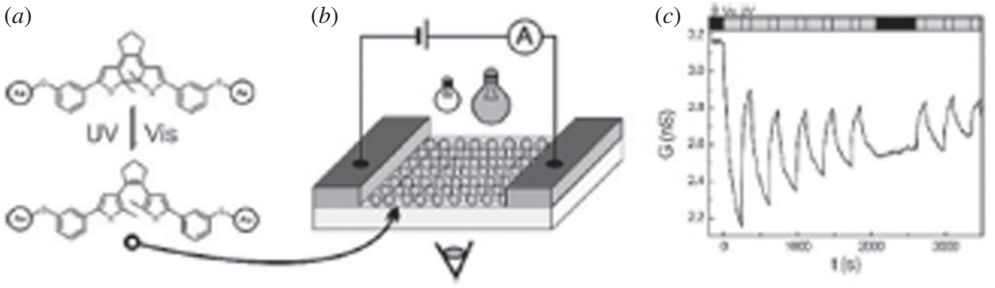

Figure 25. (*a*) Scheme of the switching molecule, a dithiolated diarylethene; top, closed form ('on' state); bottom, open form ('off' state). (*b*) Scheme of the measuring set-up for the light-induced conductance switching. (*c*) Diagram of the repeated conductance switching experiments; conductance G is plotted versus illumination time. Reprinted with permission from van der Molen *et al.* (2009). Copyright © 2009 American Chemical Society.

Upon illumination with UV light at ambient temperature, the diarylethene molecules switch from the conducting closed state ('on' state, figure 25*a*) to the non-conducting open state ('off' state, figure 25*a*), which is reflected by a rapid decrease in the conductance measurements. It was demonstrated that four conductance switching cycles can be performed before the switching molecules decomposed. The decay in the switching amplitude was explained by the fact that, at every switching process, the number of switching molecules decreased. This example represents a further interesting approach towards photochemically induced switching.

Another approach leading to densely packed, electrically conducting monolayers without the need to interconnect the nanoparticles utilizes the unique DNA Watson–Crick base pairing principle and was developed by our group (Niemeyer *et al.* 2001, 2003; Zou *et al.* 2005; Koplin *et al.* 2006). The substrate surface is first functionalized with a dendritic hyper-branched poly(amidoamine), which after activation with disuccinimidyl glutarate as the linker reagent allows the covalent attachment of 5′-aminofunctionalized DNA oligomers. Owing to specific Watson–Crick base pairing, AuNPs, functionalized with complementary oligonucleotides, are immobilized on substrate surfaces (figure 26). By using this system, particle density on the substrate surfaces up to $\geq$850 particles μm^{-2} could be achieved, as derived from AFM studies (figure 27). The arrays were characterized by I–V measurements and temperature-dependent IS. The electrical features of these layers showed pronounced field dependence as well as thermal activation of the conductivity, reflecting classical hopping transport (figure 28).

4. AuNPs in biological environments

The view on 'AuNPs in biological environments' involves the *in vitro* as well as *in vivo* applications of individual AuNPs or of AuNPs/biomolecule hybrid structures. *In vitro* applications for sensing and imaging purposes can be envisaged (Rosi & Mirkin 2005; Murphy *et al.* 2008; Jumar Ahirawal & Mitra 2009; Lin *et al.* 2009; Zhang *et al.* 2009), whereas the *in vivo* aspect is related to

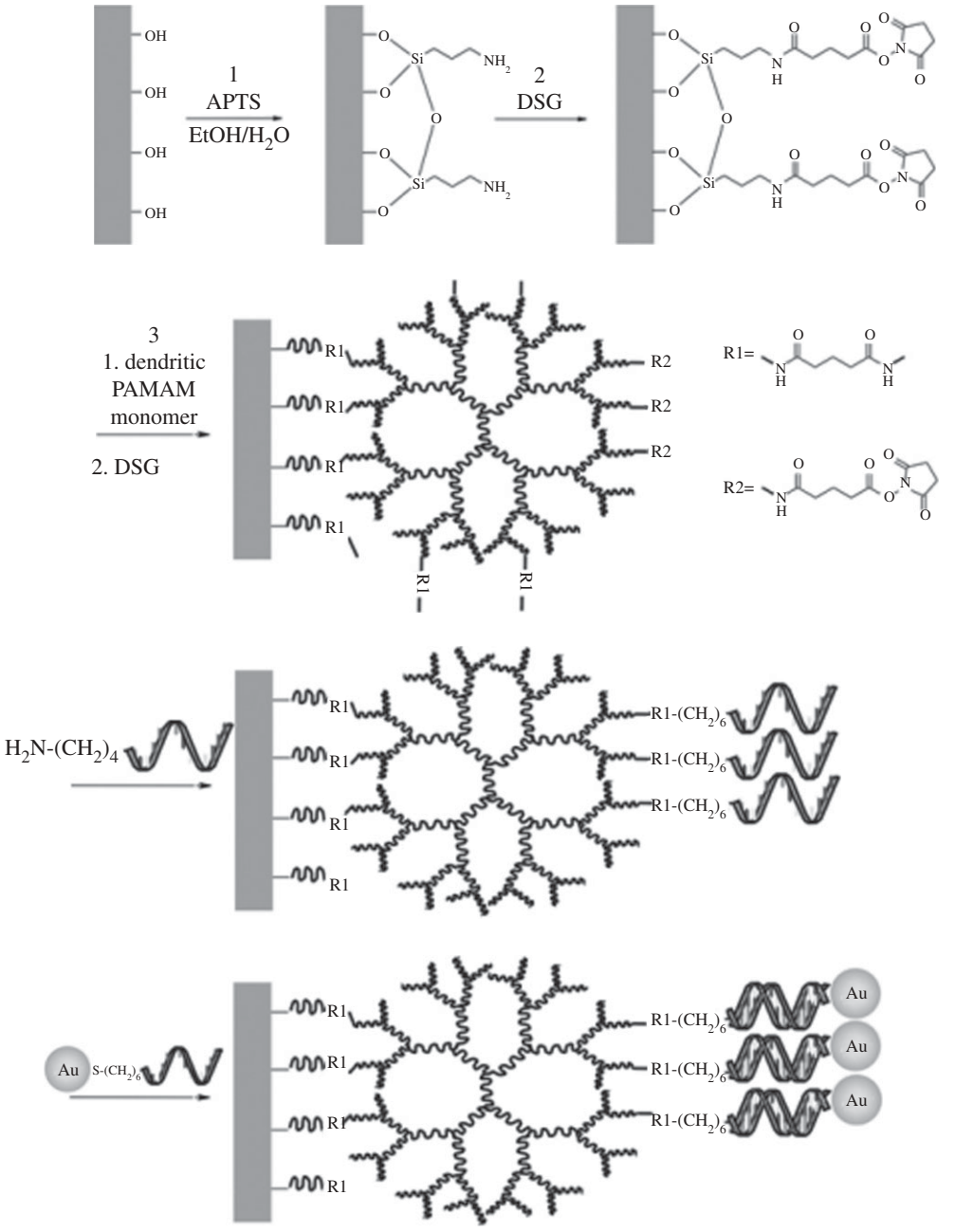

Figure 26. Schematic of the immobilization of AuNPs by DNA hybridization on silicon dioxide surfaces. Reproduced with permission from Koplin *et al.* (2006). Copyright © The Royal Society of Chemistry.

therapeutic purposes such as drug delivery (Han *et al.* 2007*b*), gene regulation (Rosi *et al.* 2006; Seferos *et al.* 2007) and cytostatics (Panyala *et al.* 2009). Recent reviews provide an extended overview on this field of research (Jain *et al.* 2008;

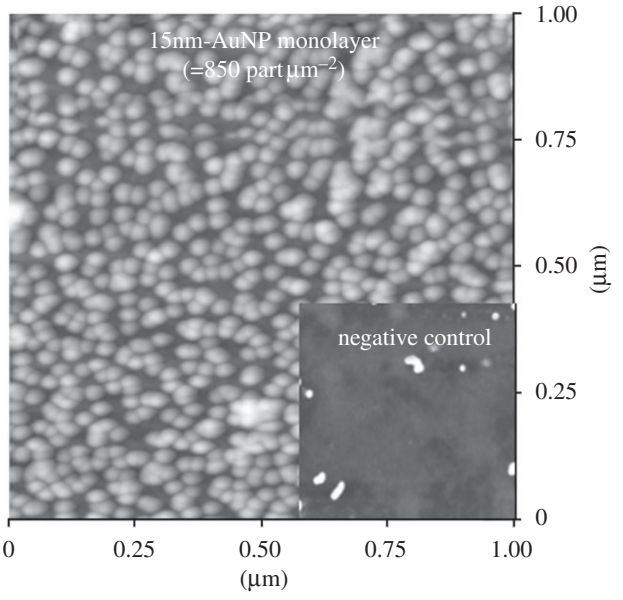

Figure 27. AFM image of a densely packed monolayer of 15 nm spherical AuNPs applying the DNA hybridization scheme as described earlier. The inset shows the topography of the control experiment with unmodified substrate surfaces.

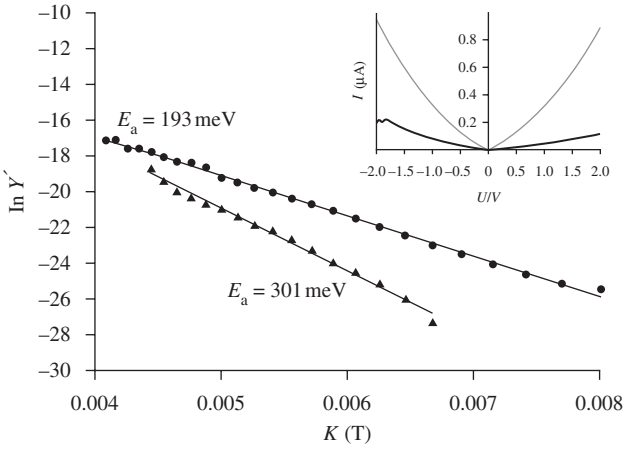

Figure 28. Arrhenius plots of samples prepared by specific (triangles) and non-specific (dots) immobilization. Inset: corresponding $I(V)$ curves for specific (grey curve) and non-specific (black curve) immobilization. Reproduced with permission from Koplin *et al.* (2006). Copyright © The Royal Society of Chemistry.

Murphy *et al.* 2008; Sperling *et al.* 2008; Wilson 2008). AuNPs of a few nanometres are of the same size range as proteins, enzymes and DNA and therefore are suitable for direct interactions with typical cellular subunits or proteins, thus enabling the preparation of novel biomolecule–nanoparticle hybrid materials. Furthermore, the SPR of AuNPs greater than 5 nm seems to be a sensory tool leading to a wide range of applications in biodiagnostics.

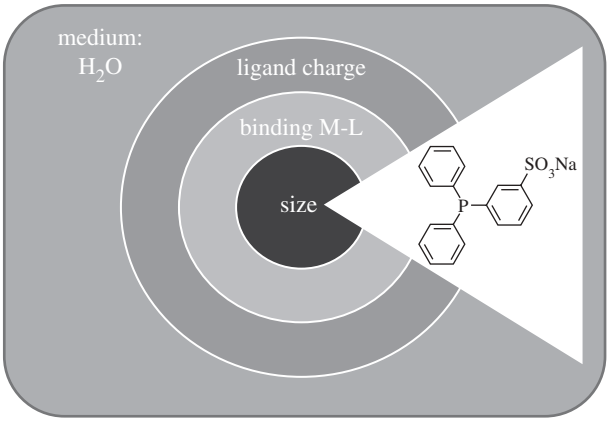

Figure 29. Parameters influencing the interaction of AuNPs in biological surroundings are the size, the nature of the ligand particle surface bonding and the nature of the 'outer' ligand shell (ligand charge).

Many of the potential *in vitro* applications of AuNPs functionalized with biomolecules rely on directed assembly. Especially the combination of DNA and AuNPs is of high relevance. DNA embodies a relatively high physico-chemical stability, and the specificity of Watson–Crick base pairing allows programmable assembly with defined spacer lengths. The multitude of binding sites at the DNA bases and the charged backbone offers many opportunities for a selective modification of the DNA with AuNPs. Furthermore, progress in DNA synthesis enables preparing and programming of artificial DNA fragments of predefined length and composition. The concept of utilizing DNA as a template for the creation of novel materials from AuNPs was introduced about a decade ago (Alivisatos *et al.* 1996; Mirkin *et al.* 1996; Mucic *et al.* 1998; Niemeyer *et al.* 1998; Mirkin 2000; Niemeyer 2001*b*; Fischler & Simon 2009).

In vivo applications lead to a fundamental question of whether there is any toxicological impact of AuNPs on cells. As mentioned before, many studies on AuNP cytotoxicity are inconsistent so far. Depending on the size and the shape of the particles as well as the nature of the ligand shell, the binding strength of the ligand to the gold surface and the functionalities in the outer sphere (figure 29) seem to play a critical role in the cellular uptake and in possible intracellular modifications and thus on cytotoxicity (Jahnen-Dechent & Simon 2008).

At this point, it is not possible to give a generalized statement about the toxicity of AuNPs. Systematic studies are under way, but they require a huge research effort owing to the large number of different control parameters (figure 29) playing a critical role in the complex interplay between nanoparticles and cells (Murphy *et al.* 2008). However, once the questions related to toxicity are answered, the path to producing highly specific drugs as well as versatile tools utilizing the unique chemical and physical properties of AuNPs, for example switching on and off distinct biomolecular pathways or selectively interacting with cellular subunits, will become clearer.

(*a*) *Cytotoxicity*

Commonly, particles greater than 10 nm are referred to as non-toxic, mostly independent of the specific ligand molecules. However, it has been reported that cetyltrimethylammonium bromide (CTAB)-stabilized gold nanorods (around 65 × 11 nm) are toxic to HeLa cells (Niidome *et al.* 2006). However, the toxic effect within these particles refers probably more to the toxicity of the stabilizing ligand itself, as the gold nanorods are stabilized by a non-covalently adsorbed bilayer of CTAB, which may desorb upon entering the cells (Connor *et al.* 2005). This fact already indicates that, despite the toxicity of the nanoparticle itself, the toxic properties depend on the binding strength of the ligand to the gold surface and have to be considered when looking for possible adverse effects.

In contrast to the larger nanoparticles, AuNPs of sizes below 2 nm showed unexpectedly high cytotoxicities in different cell lines. For example, systematic investigations of water-soluble AuNPs stabilized by TPP derivatives in the size range of 0.8–15 nm in four cell lines (HeLa cervix carcinoma epithelial cells (HeLa), SK-Mel-28 melanoma cells (SK-Mel-28), L929 mouse fibroblasts (L929) and mouse monocyte/macrophage cells (J774A1)), representing major functional cell types with barrier and phagocyte function, revealed that the small gold particles of size 1.4 nm show high toxicity comparable to that of the cytostatic drug *cisplatinum* (Pan *et al.* 2007). In the same set of measurements, the gold particles of 15 nm and Tauredon (gold thiomalate) were shown to be non-toxic at up to 60-fold and 100-fold higher concentrations, respectively (figure 30).

Furthermore, these investigations revealed that the small AuNPs of size 1.4 nm cause predominantly rapid cell death by necrosis within 12 h, whereas closely related 1.2 nm particles cause predominantly programmed cell death by apoptosis (figure 31).

In our recent studies focusing on the major cell death pathways, it was found that the cytotoxicity of 1.4 nm AuNPs was accompanied by oxidative stress, which causes mitochondrial permeability transition and triggers cell death by necrosis, and that this effect critically depends on the ligand chemistry (Pan *et al.* 2009).

In order to answer the question of whether the induced oxidative stress is an effect that results from reactive oxygen species (ROS) evolved directly from the AuNPs themselves or whether ROS production occurred secondary to AuNP cell incorporation and interaction with intracellular target molecules, a series of tests on HeLa cells applying antioxidizing compounds, either in a treatment before addition of the toxic triphenylphosphinemonosulphonate (TPPMS)-stabilized 1.4 nm AuNPs or by treating the cells with a combination of both AuNPs and antioxidizing species, were performed. Figure 32 summarizes the results obtained. The introduced antioxidizing species were *N*-acetylcysteine (NAC), glutathione (GSH), TPPMS and ascorbic acid. It became apparent that pre-treatment of the HeLa cells with the antioxidizing agents NAC, GSH, TPPMS and without washing in-between cluster addition (column D, figure 32) has a strong influence on cell survival. In contrast, ascorbic acid did not show any effect on cell survival for the entire duration of the experiments.

From this, it is suggested that either the thiol moiety or the presence of excess ligand is the reason for the reduced cell toxicity rather than the antioxidizing character of the added compounds, or that the creation of ROS directly evolving from the original reactivity of the AuNP causes the observed

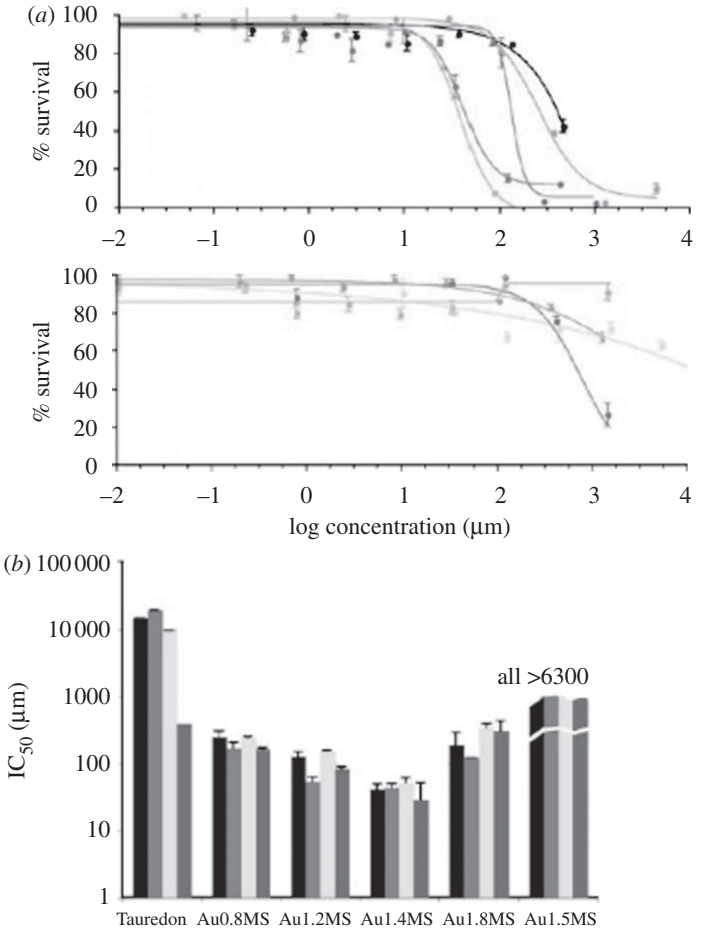

Figure 30. Cytotoxicities of Au compounds during the logarithmic growth phase of four cell lines. (*a*) HeLa cells were seeded at 2000 cells per well and grown for 3 days into the logarithmic growth phase. Au compounds were added for 48 h, and MTT tests were performed as detailed earlier. The logarithmic curve fits of tabulated MTT readings are shown. Each datum point represents the mean standard error (s.e.) of sample triplicates. Filled square, Au0.8TPPMS; open square, Au1.2TPPMS; filled triangle, Au1.4TPPMS; open triangle, Au1.4TPPTS; filled circle, Au1.8TPPMS; open circle, Au15 TPPMS; filled diamond, Tauredon; open diamond, TPPMS; cross, TPPTS. (*b*) Note that the IC_{50} values of Au1.4MS were lowest across all cell lines and that Au compounds of smaller or larger sizes were progressively less cytotoxic, which suggests a stringent size dependency of cytotoxicity. All concentrations relate to the amount of gold detected by atomic-absorption spectroscopy in the authentic samples after performing the cytotoxicity test. This procedure ruled out the possibility that cluster synthesis contaminants or dilution errors may have caused erroneous results. Black bar, HeLa; grey bar, SK-Mel-28; light grey bar, L929; dark grey bar, J774A1. Reproduced with permission from Pan *et al.* (2007). Copyright © 2007 Wiley-VCH Verlag GmbH & Co. KGaA.

cell toxicities. This latter suggestion is strongly supported by the fact that AuNPs themselves, in general, create ROS from dioxygen owing to their high surface/volume ratio (Nel *et al.* 2006) and that the closely related 1.4 nm TPP-stabilized gold clusters selectively catalyse the oxidation with O_2, both in the gas

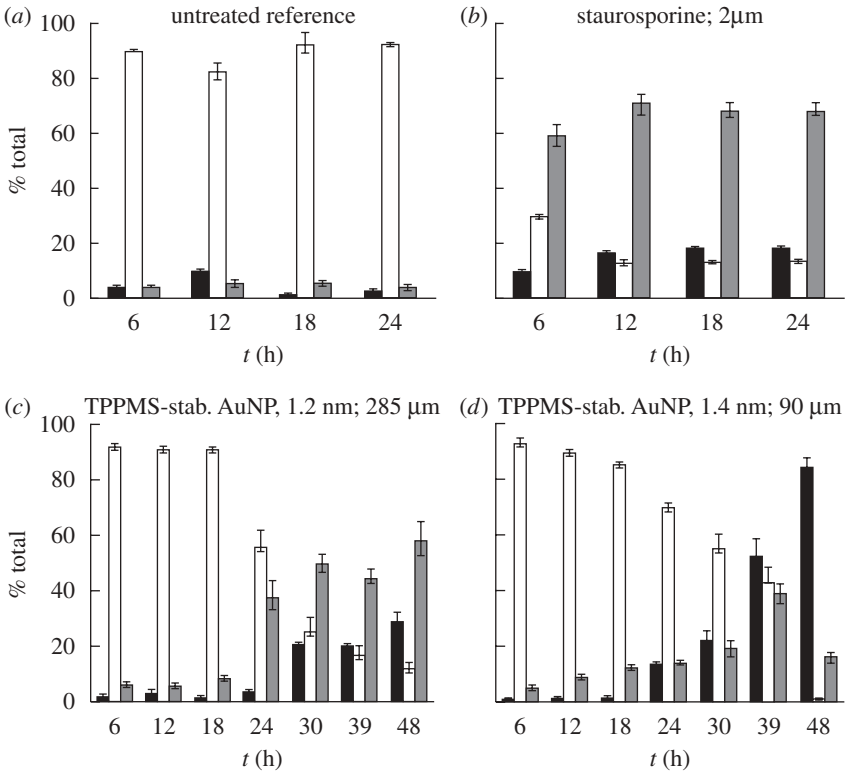

Figure 31. Determination of live, apoptotic and necrotic HeLa cells untreated or treated with the indicated compounds for 6, 12, 18 and 24 h. Cells were analysed by aV/PI double staining and flow cytometry. Depending on the material endocytosed, the HeLa cells showed no cell death (untreated, *a*), predominantly apoptosis (staurosporine, *b*), slow cell death with equal proportions of apoptosis and necrosis (*c*) or rapid cell death with transient apoptosis and predominantly necrosis (*d*). Black bar, necrotic; white bar, living; grey bar, apoptotic. Reproduced with permission from Pan *et al.* (2007). Copyright © 2007 Wiley-VCH Verlag GmbH & Co. KGaA.

phase (Turner *et al.* 2008) and in solution (Ionita *et al.* 2007). Furthermore, Au_{55} clusters reveal a remarkable stability towards oxidation (Boyen *et al.* 2002), which is most likely because of their closed-shell structure, a property that indicates that this cluster is an effective oxidation catalyst (Pina *et al.* 2008). Additionally, within the previously mentioned investigations on the selective oxidizing effect of Au_{55}, it became apparent that thiol-stabilized AuNPs were inactive in this context, which is most likely due to the strong thiolate–gold bond between the ligand and the nanoparticle's surface (Ionita *et al.* 2007). This result may further explain why upon pre-treatment of the cells with the thiol containing NAC and GSH before incubation with the nanoparticles the toxicity is reduced, i.e. due to partial ligand exchange during endocytosis resulting in the formation of strong ligand–nanoparticle bonds. Along with this, the reduced toxicity, which was observed in the presence of excess ligand (TPPMS), is a consequence of preventing ligand exchange by interacting the gold cluster core with intracellular biological compounds.

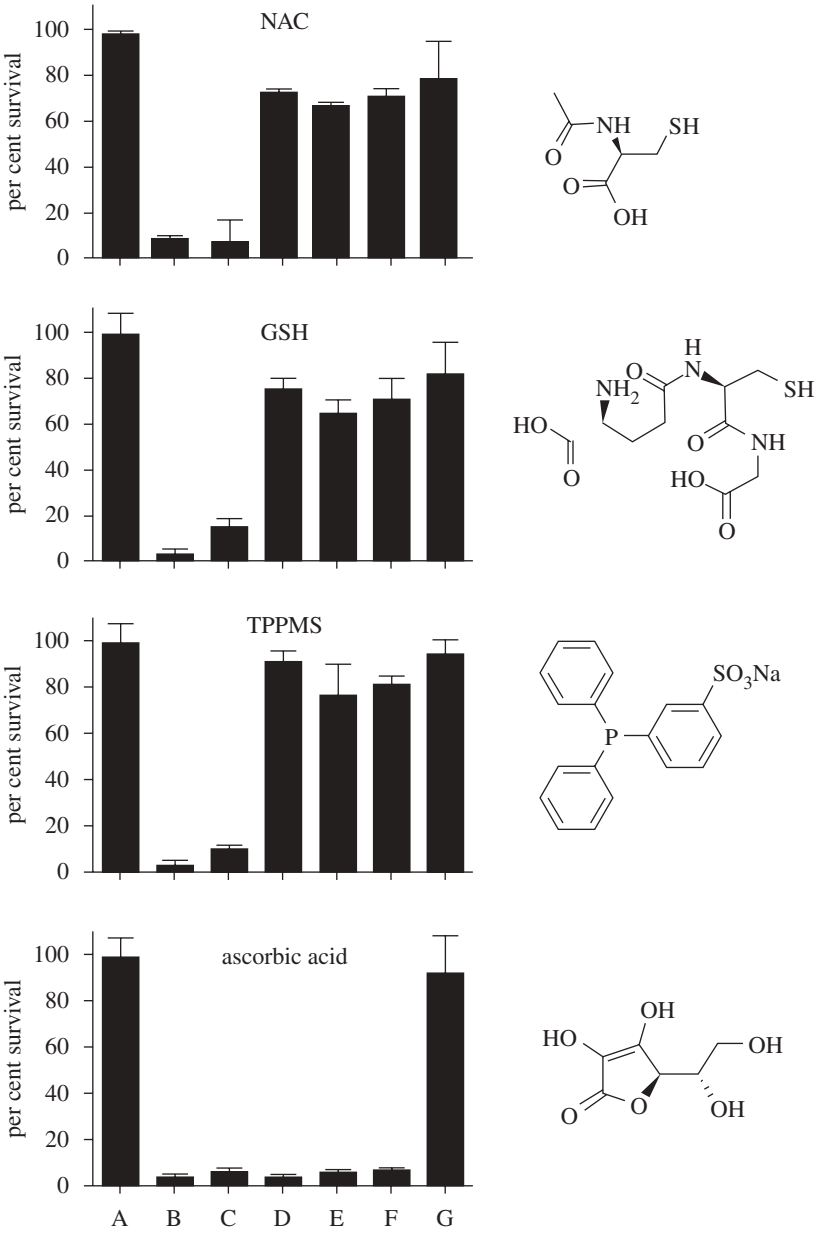

Figure 32. NAC, GSH and TPPMS but not ascorbic acid can partially inhibit the cytotoxicity of 100 µM Au1.4MS. (A) Untreated cells. (B) Cells treated with Au1.4MS for 48 h. (C) Cells pre-treated with reducing agent for 3 h, washed and post-treated with Au1.4MS for 48 h. (D) Au1.4MS pre-treated with reducing agent for 3 h, mixture added to cells for 48 h. (E) Cells pre-treated with reducing agent for 3 h, then added Au1.4MS and incubated for 48 h. (F) Reducing agent mixed with Au1.4MS and mixture immediately added to cells and incubated for 48 h. (G) Cells incubated with reducing agent for 48 h. In all cases $n = 3$; $p < 0.001$ for B/D, B/E, B/F comparisons determined by ANOVA. Reproduced with permission from Pan *et al.* (2009). Copyright © 2009 Wiley-VCH Verlag GmbH & Co. KGaA.

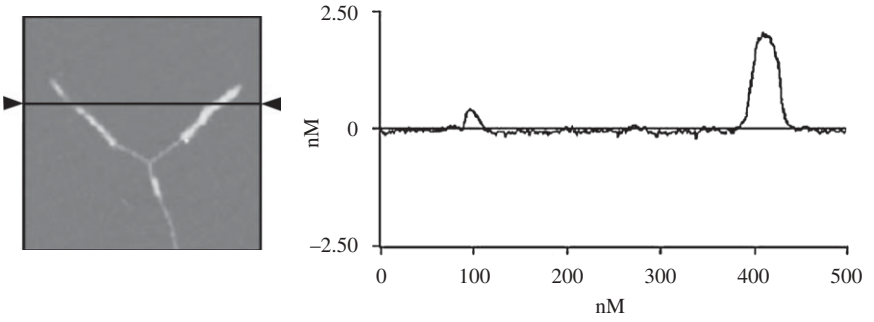

Figure 33. AFM image of a y-formed piece of B-DNA, partially covered with clusters. The cross section shows the difference in height between non-covered and covered DNA (*ca* 1.8 nm). Reproduced with permission from Liu *et al.* (2003). Copyright © 2003 Wiley-VCH Verlag GmbH & Co. KGaA.

Such interactions of TPP-stabilized Au_{55} clusters with intracellularly present biological species such as DNA have already been investigated. The treatment of natural B-DNA with Au_{55} clusters resulted in cluster decorated DNA fragments, as visible by AFM measurements (figure 33; Liu *et al.* 2003).

From molecular modelling calculations, it was deduced that the nanoparticles bind tightly to the major groove of B-DNA, which is probably due to two reasons: firstly, the size of the major grooves (figure 34), which is known from X-ray diffraction data, fits very well with the particle's size, and, secondly, the surface charge of the cluster, resulting in strong electrostatic interactions with the negatively charged phosphates of the DNA and the particle's surface.

These investigations, together with the experimental findings that approximately 20 per cent of the Au_{55} clusters taken up by the cells (Tsoli *et al.* 2005) will be finally bound to DNA, suggest that the primary cellular response is reflected by oxidative stress, followed by subsequent inhibition of DNA transcription and replication.

Furthermore, nanoparticles, in general, can stimulate the clustering of low-affinity ligands on nanoparticle scaffolds, thereby enhancing biological signalling (Jiang *et al.* 2008). The matching cellular structure may be lipid rafts on cell membranes containing receptor and transducer assemblies called signalosomes or the assembly of a low-affinity monovalent interaction that becomes a high-affinity multivalent interaction.

Altogether, these examples reveal the multitude of influencing parameters that have to be considered when thinking of an *in vivo* application of AuNPs: the size, the shape, the ligand composition involving the ligand to surface bond strength and the functionalities in the outer ligand shell and, lastly, the interaction with intracellular components along with the endocytosis.

So far, we have learnt that larger ligand-stabilized AuNPs and small thiol-stabilized gold clusters show low toxicity, which means, with view to medical applications, that these nanoparticles may be suitable for labelling, imaging and sensing applications. In contrast, small particles stabilized with weak coordinating ligands may have the potential to compete with established cytostatic drugs such as cisplatinum, whereby the advantage of the nanoparticle-based system

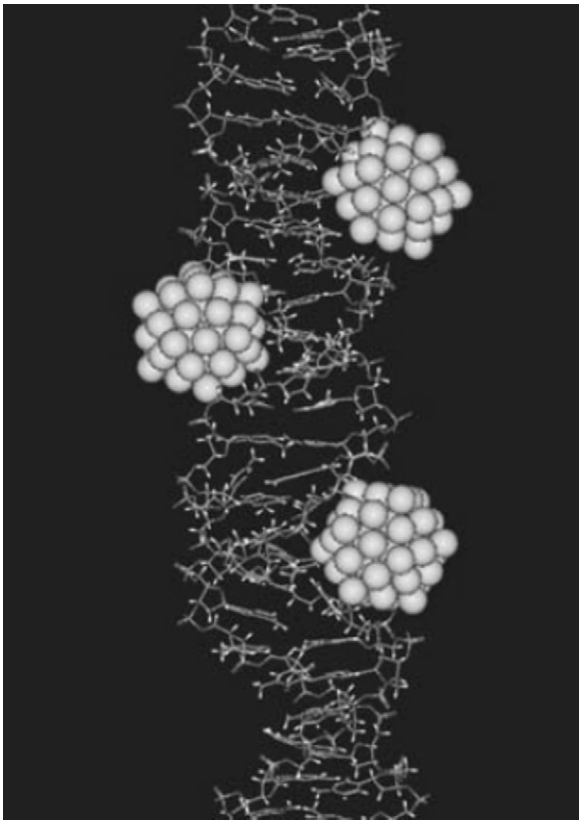

Figure 34. Modelling of the interaction of bare Au_{55} clusters with the major grooves of B-DNA. Reproduced with permission from Liu *et al.* (2003). Copyright © 2003 Wiley-VCH Verlag GmbH & Co. KGaA.

would provide chemists with huge possibilities to control the surface chemistry, which may even lead to higher specificity based on biomolecular recognition of specific cells. So, once the above-mentioned parameters are fully understood and controllable, this knowledge could be used to create new materials for specific drugs. But this is still a great challenge.

(*b*) *AuNP assemblies as sensors and actuators for biomolecular reactions*

Based on the fact that larger nanoparticles (greater than 10 nm) exhibit low toxicity in combination with the typical optical properties, new ideas have been developed for the utilization of large AuNPs for sensing and actuator purposes in biomolecular reactions.

One key control parameter for chemical reactions is the temperature. In applications in which a very local control of reactions is required, e.g. such as in molecular SA processes or lab-on-a-chip applications, it is desirable to have a fast and precise tool for manipulating the temperature at micrometre or even nanometre scales, with the presumption that the surrounding temperature should remain unaffected. Related to this task, one approach is to utilize large AuNPs as antennae for localized energy transfer.

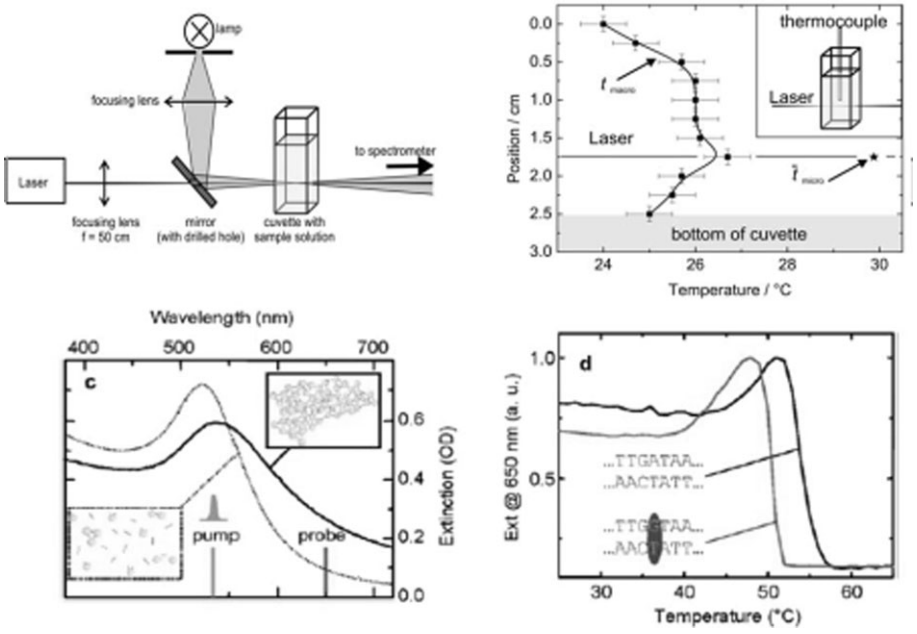

Figure 35. (*a*) Experimental set-up for the laser-induced melting of AuNP–DNA networks by Reismann *et al.* (2008). Reproduced with permission from Reismann *et al.* (2008). Copyright © 2008 Wiley-VCH Verlag GmbH & Co. KGaA. (*b*) The black squares show the vertical profile of temperature in the unirradiated region of the network suspension, t_{macro}, during laser irradiation ($I = 5\,\mathrm{kW\,cm^{-2}}$). The star shows the microscopic temperature, μ_{t}, in the irradiated region as determined by the interferometric measurement. For clarity, the vertical positions of the bottom of the cuvette and the laser beam path are illustrated. Inset: sketch of the sample cuvette with the thermocouple and the position of the laser beam path, thereby showing that the heating is locally defined. Reproduced with permission from Reismann *et al.* (2008). Copyright © 2008 Wiley-VCH Verlag GmbH & Co. KGaA. (*c*) Extinction curves of DNA-bound AuNPs as aggregates at 25°C (solid line) and after laser-induced melting of the networks at 60°C (dotted line) showing the shift and the broadening of the plasmon resonance peak in the experiment by Stehr *et al.* (2008). The wavelengths of the pump and the probe laser are marked. (*d*) The experiment allows for discrimination between perfectly matching DNA duplexes and those with single base mismatches. Reprinted with permission from Stehr *et al.* (2008). Copyright © 2008 American Chemical Society.

Hamad-Schifferli *et al.* (2002) first investigated the energy transfer on AuNP–DNA conjugates. They utilized 1.4 nm AuNPs to trigger the dehybridization of a DNA hairpin structure. The principle is based on the fact that, upon inductive coupling with a radio-frequency magnetic field, the AuNP heats up and induces melting of the covalently attached hairpin DNA structure. Most recently, we have demonstrated the laser-induced photothermal melting of AuNP–DNA networks in solution (Reismann *et al.* 2008). In this experiment, the DNA dehybridization in the networks was induced by laser excitation of the surface plasmon of the AuNPs, which was converted into heat and consequently led to a heat transfer from the particles' surface into the covalently attached DNA. The photothermally

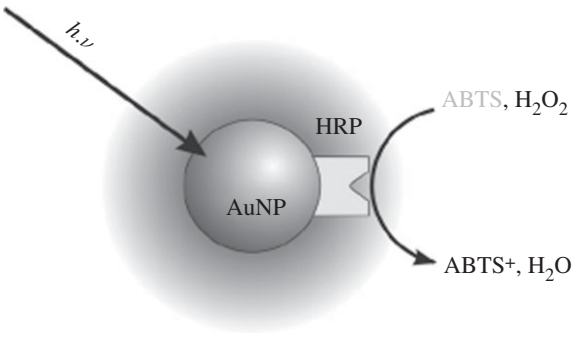

Figure 36. Principle of the photothermal experiment. HRP is bound to the surface of an AuNP. Laser light is absorbed by the AuNP and transformed into heat, which dissipates into the environment of the nanoparticle. This heat influences the enzymatic conversion of ABTS and H_2O_2 to $ABTS^+$ and H_2O, respectively. Reproduced with permission from Bretschneider *et al.* (2009). Copyright © 2009 Wiley-VCH Verlag GmbH & Co. KGaA.

induced melting process was followed spectroscopically by means of UV–Vis. The set-up of the experiment is shown in figure 35*a*. It is worth noting that this process is locally confined to the dimensions of the laser beam, i.e. the illuminated volume, leaving the environment unaffected (figure 35*b*) and thus giving the prospect of a future application in targeted drug delivery systems, if the utilized laser wavelength (near infrared) lies in the optically transparent window of tissue.

A further approach based on the same principle was presented by Stehr *et al.* (2008), who investigated the melting of DNA–nanoparticle networks on a microsecond time scale by means of 300 ns laser pulses (figure 35*c*). The melting transition of such 'gold nanostoves' could be used to distinguish between perfectly matching double strands and those with a single base pair mismatch in an extremely short time window, as shown in figure 35*d*. Compared with the previous methods, the advantage of this method is the acceleration, i.e. the short read out time of less than a millisecond and the circumvention of heating ramps as in conventional DNA melting assays.

The photothermal melting of DNA networks can also be regarded as the first approach towards remote-controlled activation of biomolecular reactions, such as the enzymatic conversion of molecules. In this context, our group very recently demonstrated that the activity of horseradish peroxidase (HRP), bound to the surface of 15 nm AuNPs (figure 36), can be controlled through laser irradiation at a wavelength of 532 nm (Bretschneider *et al.* 2009).

The irradiation results in the deactivation of the enzyme, whose rate increases with increasing laser power. This deactivation can be observed *in situ* by UV–Vis spectroscopy.

This is an example of a photothermally controlled bioreaction that involves enzymatic conversion on the surface of AuNPs. Based on these results, one can envision photothermal control in more complex reaction systems even in cells or tissues, where photothermal treatment might allow them to temporally and spatially manipulate a particular species in the mixture.

5. Conclusion

In summary, we have collected some recent examples of research on AuNPs, which are directed towards applications in nanoelectronics, biology or medicine. While most of the size-dependent properties of AuNPs have repeatedly been treated in previous reviews or book chapters, this review should shed light on very recent progress in this field, whereby we put emphasis on our own work. It would by far exceed the frame of such a short review article to reflect the current state of knowledge *in toto*; thus, our aim was to present a collection of examples, which, in our opinion, brought something new into the field.

In nanoelectronic applications, it is still a great challenge to assemble AuNPs into highly ordered and defect-free arrangements, which would allow precise control of sequential tunnelling or SCS. As illustrated by the examples chosen here, we believe that applications in a technical device require convergence of molecular assembly and nanoelectrode fabrication. This can be achieved only by interdisciplinary efforts from chemistry and electrical engineering, but it is worth trying because SE based on chemically tailored nanoparticles might have the chance to become a reliable technology in the post-CMOS area.

In biomedical applications, the novel concepts of size-dependent toxicity, selection of reaction pathways in cell toxicity as well as approaches towards remote control of biomolecular reactions on the surface of AuNPs may pave the way to new fields in nanomedicine. The vision of selective drugs, e.g. for cancer therapy or the controlled intracellular release of drugs, DNA or RNA is becoming clearer and may fuel a growing field of research, the progress of which will critically depend on interdisciplinary research efforts, jointly driven by experts from chemistry, physics, biology and medicine.

The authors thank the Jülich-Aachen-Research-Alliance (JARA) section Fundamentals of Future Information Technology (FIT) and the German Research Foundation (DFG) for financial support.

References

Albrecht, T., Mertens, S. F. L. & Ulstrup, J. 2007 Intrinsic multistate switching of gold clusters through electrochemical gating. *J. Am. Chem. Soc.* **129**, 9162–9167. (doi:10.1021/ja072517h)

Alivisatos, A. P. 1996 Semiconductor clusters, nanocrystals, and quantum dots. *Science* **271**, 933–937. (doi:10.1126/science.271.5251.933)

Alivisatos, A. P., Johnsson, K. P., Peng, X., Wilson, T. E., Loweth, C. J., Bruchez Jr, M. P. & Schultz, P. G. 1996 Organization of 'nanocrystal molecules' using DNA. *Nature* **382**, 609–611. (doi:10.1038/382609a0)

Bates, A. D. *et al.* 2006 Construction and characterization of a gold nanoparticle wire assembled using Mg^{2+}-dependent RNA-RNA interactions. *Nano Lett.* **6**, 445–448. (doi:10.1021/nl052316g)

Bezryadin, A., Dekker, C. & Schmid, G. 1997 Electrostatic trapping of single conducting nanoparticles between nanoelectrodes. *Appl. Phys. Lett.* **71**, 1273. (doi:10.1063/1.119871)

Blech, K., Noyong, M., Juillerat, F., Nakayama, T., Hofmann, H. & Simon, U. 2008 *In-situ* electrical addressing of one-dimensional gold nanoparticle assemblies. *J. Nanosci. Nanotechnol.* **8**, 461. (doi:10.1166/jnn.2008.192)

Boisselier, E. & Astruc, D. 2009 Gold nanoparticles in nanomedicine: preparations, imaging, diagnostics, therapies and toxicity. *Chem. Soc. Rev.* **38**, 1759–1782. (doi:10.1039/b806051g)

Boyen, H. *et al.* 2002 Oxidation-resistant gold-55 clusters. *Science* **297**, 1533. (doi:10.1126/science.1076248)

Braun, G., Inagaki, K., Estabrook, R. A., Wood, D. K., Levy, E., Cleland, A. N., Strouse, G. F. & Reich, N. O. 2005 Gold nanoparticle decoration of DNA on silicon. *Langmuir* **21**, 10 699–10 701. (doi:10.1021/la0515367)

Bretschneider, J. C., Reismann, M., von Plessen, G. & Simon, U. 2009 Photothermal control of the activity of HRP-functionalized gold nanoparticles. *Small* **5**, 2549–2553. (doi:10.1002/smll.200900544)

Briant, C. E., Theobald, B. R. C., White, J. W., Bell, L. K. & Mingos, D. M. P. 1981 Synthesis and *X*-ray structural characterization of the centred icosahedral gold cluster compound $[Au_{13}(PMe_2Ph)_{10}Cl_2](PF_6)_3$; the realization of a theoretical prediction. *J. Chem. Soc. Chem. Commun.* 201. (doi:10.1039/c39810000201)

Brousseau III, L. C., Zhao, Q., Schultz, D. A. & Feldheim, D. L. 1998 pH-gated single-electron tunneling in chemically modified gold nanoclusters. *J. Am. Chem. Soc.* **120**, 7645–7646. (doi:10.1021/ja981262s)

Brune, H. *et al.* 2006 *Nanotechnology.* Weinheim, Germany: Springer.

Brust, M., Walker, M., Bethell, D., Schiffrin, D. J. & Whyman, R. 1994 Synthesis of thiol-derivatised gold nanoparticles in a two-phase liquid–liquid system. *J. Chem. Soc. Chem. Commun.* 801–802. (doi:10.1039/c39940000801)

Brust, M., Fink, J., Bethell, D., Schiffrin, D. J. & Kiely, C. 1995 Synthesis and reactions of functionalised gold nanoparticles. *J. Chem. Soc. Chem. Commun.* 1655–1656. (doi:10.1039/c39950001655)

Buffat, Ph. & Borel, J.-P. 1976 Size effect on the melting temperature of gold particles. *Phys. Rev. A* **13**, 2287–2298. (doi:10.1103/PhysRevA.13.2287)

Burda, C., Chen, X., Narayanan, R. & El-Sayed, M. A. 2005 Chemistry and properties of nanocrystals of different shapes. *Chem. Rev.* **105**, 1025–1102. (doi:10.1021/cr030063a)

Castro, T., Reifenberger, R., Choi, E. & Andres, R. P. 1990 Size-dependent melting temperature of individual nanometer-sized metallic clusters. *Phys. Rev. B* **42**, 8548–8556. (doi:10.1103/PhysRevB.42.8548)

Chen, C.-F., Tzeng, S.-D., Chen, H.-Y., Lin, K.-J. & Gwo, S. 2008 Tunable plasmonic response from alkanethiolate-stabilized gold nanoparticle superlattices: evidence of near-field coupling. *J. Am. Chem. Soc.* **130**, 824–826. (doi:10.1021/ja0773610)

Chi, L. F., Hartig, M., Drechsler, T., Schaak, Th., Seidel, C., Fuchs, H. & Schmid, G. 1998 Single-electron tunneling in Au_{55} cluster monolayers. *Appl. Phys. Lett. A* **66**, 187. (doi:10.1007/s003390051127)

Collier, C. P., Sayhally, R. J., Shiang, J. J., Henricks, S. E. & Heath, J. R. 1997 Reversible tuning of silver quantum dot monolayers through the metal–insulator transition. *Science* **277**, 1978–1981. (doi:10.1126/science.277.5334.1978)

Collier, C. P., Vossmeyer, T. & Heath, J. R. 1998 Nanocrystal superlattices. *Annu. Rev. Phys. Chem.* **49**, 371–404. (doi:10.1146/annurev.physchem.49.1.371)

Connor, E. E., Mwamuka, J., Gole, A., Murphy, C. J. & Wyatt, M. D. 2005 Gold nanoparticles are taken up by human cells but do not cause acute cytotoxicity. *Small* **1**, 325–327. (doi:10.1002/smll.200400093)

Corma, A. & Garcia, H. 2008 Supported gold nanoparticles as catalysts for organic reactions. *Chem. Soc. Rev.* **37**, 2096–2126. (doi:10.1039/b707314n)

Coskun, U. C. *et al.* 2008 Single-electron transistors made by chemical patterning of silicon dioxide substrates and selective deposition of gold nanoparticles. *Appl. Phys. Lett.* **93**, 123 101. (doi:10.1063/1.2981705)

Cui, Y., Jörk, M. T., Liddlem, J. A., Sönnichen, C., Boussert, B. & Alivisatos, A. P. 2004 Integration of colloidal nanocrystals into lithographically patterned devices. *Nano Lett.* **4**, 1093. (doi:10.1021/nl049488i)

Daniel, M.-C. & Astruc, D. 2004 Gold nanoparticles: assembly, supramolecular chemistry, quantum-size-related properties, and applications toward biology, catalysis, and nanotechnology. *Chem. Rev.* **104**, 293–346. (doi:10.1021/cr030698+)

Deng, Z., Tian, Y., Lee, S., Ribbe, A. E. & Mao, C. 2005*a* DNA-encoded self-assembly of gold nanoparticles into one-dimensional arrays. *Angew. Chem. Int. Ed.* **44**, 3582–3585. (doi:10.1002/anie.200463096)

Deng, Z., Tian, Y., Lee, S., Ribbe, A. E. & Mao, C. 2005*b* DNA-encoded self-assembly of gold nanoparticles into one-dimensional arrays. *Angew. Chem.* **117**, 3648–3651. (doi:10.1002/ange.200463096)

El-Ansary, A. & Al-Daihan, S. 2009 On the toxicity of therapeutically used nanoparticles: an overview. *J. Toxicol.* **2009**, 754 810.

Eustis, S. & El-Sayed, M. A. 2006 Why gold nanoparticles are more precious than pretty gold: noble metal surface plasmon resonance and its enhancement of the radiative and nonradiative properties of nanocrystals of different shapes. *Chem. Soc. Rev.* **35**, 209–217. (doi:10.1039/b514191e)

Fischler, M. & Simon, U. 2009 Metal nanoparticle–DNA hybrids—from assembly towards functional conjugates. *J. Mater. Chem.* **19**, 1518–1523. (doi:10.1039/b812225c)

Fischler, M., Simon, U., Nir, H., Eichen, Y., Burley, E. A., Gierlich, J., Gramlich, P. M. E. & Carell, Th. 2007 Formation of bimetallic Ag–Au nanowires by metallization of artificial DNA duplexes. *Small* **3**, 1049–1055. (doi:10.1002/smll.200600534)

Fischler, M., Sologubenko, A., Mayer, J., Clever, G., Burley, G. A., Gierlich, J., Carell, T. & Simon, U. 2008 Chain-like assembly of gold nanoparticles on artificial DNA templates *via* click chemistry. *Chem. Commun.* 169–171. (doi:10.1039/b715602b)

Fischler, M., Homberger, M. & Simon, U. 2009 DNA-mediated assembly of metal nanoparticles: fabrication, structural features and electrical properties. In *Nanobioelectronics—for electronics, biology, and medicine* (eds A. Offenhäusser & R. Rinaldi), pp. 11–41. New York, NY: Springer.

Franke, M. E., Koplin, T. J. & Simon, U. 2006 Metal and metal oxide nanoparticles in chemiresistors: does the nanoscale matter? *Small* **2**, 36–50. (doi:10.1002/smll.200500261)

Gierlich, J., Gutsmiedl, K., Gramlich, P. M. E., Schmidt, A., Burley, G. A. & Carell, T. 2007 Synthesis of highly modified DNA by a combination of PCR with alkyne-bearing triphosphates and click chemistry. *Chem. Eur. J.* **13**, 9486–9494. (doi:10.1002/chem.200700502)

Gittins, D. I., Bethell, D., Schiffrin, D. J. & Nichols, R. J. 2000 A nanometre-scale electronic switch consisting of a metal cluster and redox-addressable groups. *Nature* **408**, 67–69. (doi:10.1038/35040518)

Grabert, H. 1991 Single charge tunneling: a brief introduction. *Z. Phys. B* **85**, 319.

Grzelczak, M., Pérez-Juste, J., Mulvaney, P. & Liz-Marzán, L. M. 2008 Shape control in gold nanoparticle synthesis. *Chem. Soc. Rev.* **37**, 1783–1791. (doi:10.1039/b711490g)

Häkkinen, H. 2008 Atomic and electronic structure of gold clusters: understanding flakes, cages and superatoms from simple concepts. *Chem. Soc. Rev.* **37**, 1847–1859. (doi:10.1039/b717686b)

Häkkinen, H., Walter, M. & Grönbeck, H. 2006 Divide and protect: capping gold nanoclusters with molecular gold-thiolate rings. *J. Phys. Chem. B* **110**, 9927–9931. (doi:10.1021/jp0619787)

Halperin, W. P. 1986 Quantum size effects in metal particles. *Rev. Mod. Phys.* **58**, 533–606. (doi:10.1103/RevModPhys.58.533)

Hamad-Schifferli, K., Schwartz, J. J., Santos, A. T., Zhang, S. & Jacobson, J. M. 2002 Remote electronic control of DNA hybridization through inductive coupling to an attached metal nanocrystal antenna. *Nature* **415**, 152–155. (doi:10.1038/415152a)

Han, G., Ghosh, P. & Rotello V. M. 2007*a* Multi-functional gold nanoparticles for drug delivery. *Adv. Exp. Med. Biol.* **620**, 48–56. (doi:10.1007/978-0-387-76713-0_4)

Han, G., Ghosh, P. & Rotello, V. M. 2007*b* Functionalized gold nanoparticles for drug delivery. *Nanomedicine* **2**, 113–123. (doi:10.2217/17435889.2.1.113)

Houbertz, R., Feigenspan, T., Mielke, F., Memmert, U., Hartmann, U., Simon, U., Schön, G. & Schmid, G. 1994 STM investigations on compact Au_{55} cluster pellets. *Europhys. Lett.* **29**, 641. (doi:10.1209/0295-5075/28/9/005)

Hu, M.-S., Chen, H.-L., Shen, C.-H., Hong, L.-S., Huang, B.-R., Chen, K.-H. & Che, L.-C. 2006 Photosensitive gold-nanoparticle-embedded dielectric nanowires. *Nat. Mater.* **5**, 102–106. (doi:10.1038/nmat1564)

Ionita, P., Conte, M., Gilbert, B. & Chechik, V. 2007 Gold nanoparticle-initiated free radical oxidations and halogen abstractions. *Org. Biomol. Chem.* **5**, 3504. (doi:10.1039/b711573c)

Jadzinsky, P. D., Calero, G., Ackerson, C. J., Bushnell, D. A. & Kornberg, R. D. 2007 Structure of a thiol monolayer-protected gold nanoparticle at 1.1 Å resolution. *Science* **318**, 430–433. (doi:10.1126/science.1148624)

Jahnen-Dechent, W. & Simon, U. 2008 Function follows form: shape complementarity and nanoparticle toxicity. *Nanomedicine* **3**, 601–603. (doi:10.2217/17435889.3.5.601)

Jain, P. K., Huang, X., El-Sayed, I. H. & El-Sayed, M. A. 2008 Noble metals on the nanoscale: optical and photothermal properties and some applications in imaging, sensing, biology, and medicine. *Acc. Chem. Res.* **41**, 1578–1586. (doi:10.1021/ar7002804)

Janes, D. B., Kolagunta, V. R., Osifchin, R. G., Bielefeld, J. D., Andres, R. P., Henderson, J. I. & Kubiak, C. P. 1995 Electronic conduction through 2D arrays of nanometer diameter metal clusters. *Superlattices Microstruct.* **18**, 275–281. (doi:10.1006/spmi.1995.1112)

Jiang, W., Kim, B. Y. S., Rutka, J. T. & Chan, W. C. W. 2008 Nanoparticle-mediated cellular response is size-dependent. *Nat. Nanotechnol.* **3**, 145–150. (doi:10.1038/nnano.2008.30)

Jumar Ahirawal, G. & Mitra, C. K. 2009 Direct electrochemistry of horse radish peroxidase-gold nanoparticles conjugate. *Sensors* **9**, 881–894. (doi:10.3390/390200881)

Khanna, S. N. & Jena, P. 1992 Assembling crystals from clusters. *Phys. Rev. Lett.* **69**, 1664. (doi:10.1103/PhysRevLett.69.1664)

Kieley, C. J., Fink, J., Brust, M., Bethell, D. & Shiffrin, D. J. 1998 Spontaneous ordering of bimodal ensembles of nanoscopic gold clusters. *Nature* **396**, 444–446. (doi:10.1038/24808)

Klein, D. L., McEuen, O. L., Bowenkatari, J. E., Roth, R. & Alivisatos, A. P. 1996 An approach to electrical studies of single nanocrystals. *Appl. Phys. Lett.* **68**, 2574. (doi:10.1063/1.116188)

Klein, D. L., Roth, R., Lim, A., Alivisatos, A. P. & McEuen, P. L. 1997 A single-electron transistor made from a cadmium selenide nanocrystal. *Nature* **389**, 699–701. (doi:10.1038/39535)

Koplin, E. & Simon, U. 2007 Application of metal nanoclusters in nanoelectronics. In *Metal nanoparticles in catalysis and materials science: the issue of size control* (eds B. Corain, G. Schmid & H. Toshima), pp. 107–128. Weinheim, Germany: Elsevier Science & Technology.

Koplin, E., Niemeyer, C. M. & Simon, U. 2006 Formation of electrically conducting DNA-assembled gold nanoparticle monolayers. *J. Mater. Chem.* **16**, 1338–1344. (doi:10.1039/b516257b)

Korotkov, A. & Nazarov, Yu. 1991 Single-electron tunneling coexisting with the barrier suppression. *Physica B* **173**, 217. (doi:10.1016/0921-4526(91)90083-Q)

Laaksonen, T., Ruiz, V., Liljerothc, P. & Quin, B. M. 2008 Quantised charging of monolayer-protected nanoparticles. *Chem. Soc. Rev.* **37**, 1836–1846. (doi:10.1039/b713681c)

Le, J. D., Pinto, Y., Seeman, N. C., Musier-Forsyth, K., Taton, T. A. & Kiehl, R. A. 2004 DNA-templated self-assembly of metallic nanocomponent arrays on a surface. *Nano Lett.* **4**, 2343–2347. (doi:10.1021/nl048635+)

Lee, J.-H., Cheon, J., Lee, S. B., Chang, Y.-W., Kim, S.-I. & Yoo, K.-H. 2005 DNA linker controlled single electron tunneling behavior of nanoparticle assembly. *J. Appl. Phys.* **98**, 084 315. (doi:10.1063/1.2103411)

Li, H., Park, S. H., Reif, J. H., LaBean, T. H. & Yan, H. 2004 DNA-templated self-assembly of protein and nanoparticle linear arrays. *J. Am. Chem. Soc.* **126**, 418–419. (doi:10.1021/ja0383367)

Li, L., Gattass, R. R., Gershgoren, E., Hwang, H. & Fourkas, J. T. 2009 Achieving $\lambda/20$ resolution by one-color initiation and deactivation of polymerization. *Science* **324**, 910–913. (doi:10.1126/science.1168996)

Liao, J., Bernard, L., Langer, M., Schönenberger, C. & Calame, M. 2006 Reversible formation of molecular junctions in 2D nanoparticle arrays. *Adv. Mater.* **18**, 2444. (doi:10.1002/adma.200601001)

Lide, D. R. 1995 *Handbook of chemistry and physics.* Danvers, MA: CRC Press.

Likharev, K. K. 1987 Single-electron transistors: electrostatic analogs of the DC SQUIDS. *IEEE Trans. Magn.* **23**, 1142. (doi:10.1109/TMAG.1987.1065001)

Likharev, K. K. 1988 Correlated discrete transfer of single electrons in ultra small tunnel junctions. *IBM J. Res. Develop.* **32**, 144–157.

Lin, C.-A. J. *et al.* 2009 Synthesis, characterization, and bioconjugation of fluorescent gold nanoclusters toward biological labeling applications. *ACS Nano* **3**, 395–401. (doi:10.1021/nn800632j)

Liu, S., Maoz, R., Schmid, G. & Sagiv, J. 2002 Template guided self-assembly of [Au_{55}] clusters on nanolithographically defined monolayer patterns. *Nano Lett.* **2**, 1055. (doi:10.1021/nl025659c)

Liu, Y., Meyer-Zaika, W., Franzka, S., Schmid, G., Tsoli, M. & Kuhn, H. 2003 Gold-cluster degradation by the transition of B-DNA into A-DNA and the formation of nanowires. *Angew. Chem. Int. Ed.* **42**, 2853. (doi:10.1002/anie.200250235)

Lopez-Acevedo, O., Akola, J., Whetten, R. L., Grönbeck, H. & Häkkinen, H. 2009 Structure and bonding in the ubiquitous icosahedral metallic gold cluster $Au_{144}(SR)_{60}$. *J. Phys. Chem. C* **113**, 5035–5038. (doi:10.1021/jp8115098)

Love, J. C., Estroff, L. A., Kriebel, J. K., Nuzzo, R. G. & Whitesides, G. M. 2005 Self-assembled monolayers of thiolates on metals as a form of nanotechnology. *Chem. Rev.* **105**, 1103–1169. (doi:10.1021/cr0300789)

Loweth, C. J., Caldwell, W. B., Peng, X., Alivisatos, A. P. & Schultz, P. G. 1999*a* DNA-based assembly of gold nanocrystals. *Angew. Chem. Int. Ed.* **38**, 1808–1812. (doi:10.1002/(SICI)1521-3773(19990614)38:12%3C1808::AID-ANIE1808%3E3.0.CO;2-C)

Loweth, C. J., Caldwell, W. B., Peng, X., Alivisatos, A. P. & Schultz, P. G. 1999*b* DNA als Gerüst zur Bildung von Aggregaten aus Gold-Nanokristallen. *Angew. Chem.* **111**, 1925–1929. (doi:10.1002/(SICI)1521-3757(19990614)111:12%3C1925::AID-ANGE1925%3E3.0.CO;2-2)

Mertens, S. F. L., Blech, K., Sologubenko, A. S., Mayer, J., Simon, U. & Wandlowski, Th. 2009 Quantised double layer charging of monolayer-protected clusters in a room temperature ionic liquid. *Electrochim. Acta* **54**, 5006–5010. (doi:10.1016/j.electacta.2009.02.051)

Mirkin, C. A. 2000 Programming the assembly of two- and three-dimensional architectures with DNA and nanoscale inorganic building blocks. *Inorg. Chem.* **39**, 2258–2272. (doi:10.1021/ic991123r)

Mirkin, C. A., Letsinger, R. L., Mucic, R. C. & Storhoff, J. J. 1996 A DNA-based method for rationally assembling nanoparticles into macroscopic materials. *Nature* **382**, 607–609. (doi:10.1038/382607a0)

Mucic, R. C., Storhoff, J. J., Mirkin, C. A. & Letsinger, R. L. 1998 DNA-directed synthesis of binary nanoparticle network materials. *J. Am. Chem. Soc.* **120**, 12 674–12 675. (doi:10.1021/ja982721s)

Murphy, C. J., Gole, A. M., Stone, J. W., Sisco, P. N., Alkilany, A. M., Goldsmith, E. C. & Baxter, S. C. 2008 Gold nanoparticles in biology: beyond toxicity to cellular imaging. *Acc. Chem. Res.* **41**, 1721–1730. (doi:10.1021/ar800035u)

Murray, R. W. 2008 Nanoelectrochemistry: metal nanoparticles, nanoelectrodes, and nanopores. *Chem. Rev.* **108**, 2688–2720. (doi:10.1021/cr068077e)

Murray, C. B., Norris, D. J. & Bawendi, M. G. 1993 Synthesis and characterization of nearly monodisperse CdE (E = sulfur, selenium, tellurium) semiconductor nanocrystallites. *J. Am. Chem. Soc.* **115**, 8706–8715. (doi:10.1021/ja00072a025)

Murray, C.-B., Kayan, C. R. & Bawendi, M. G. 1995 Self-organization of CdSe nanocrystallites into three-dimensional quantum dot superlattices. *Science* **270**, 1335–1338. (doi:10.1126/science.270.5240.1335)

Myroshnychenko, V., Rodríguez-Fernández, J., Pastoriza-Santos, I., Funston, A. M., Novo, C., Mulvaney, P., Liz-Marzán, L. M. & Garcá de Abajo, F. J. 2008 Modelling the optical response of gold nanoparticles. *Chem. Rev.* **37**, 1792–1805. (doi:10.1039/b711486a)

Nel, A., Xia, T., Madler, L. & Li, N. 2006 Toxic potential of materials at the nanolevel. *Science* **311**, 622. (doi:10.1126/science.1114397)

Niemeyer, C. M. 2001*a* Bioorganic applications of semisynthetic DNA–protein conjugates. *Chem. Eur. J.* **7**, 3188–3195. (doi:10.1002/1521-3765(20010803)7:15%3C3188::AID-CHEM3188%3E3.0.CO;2-C)

Niemeyer, C. M. 2001*b* Nanoparticles, proteins, and nucleic acids: biotechnology meets materials science. *Angew. Chem. Int. Ed.* **40**, 4128–4158. (doi:10.1002/1521-3773(20011119)40:22%3C4128::AID-ANIE4128%3E3.0.CO;2-S)

Niemeyer, C. M. & Simon, U. 2005 DNA-based assembly of metal nanoparticles. *Eur. J. Inorg. Chem.* **18**, 3641–3655. (doi:10.1002/ejic.200500425)

Niemeyer, C. M., Buerger, W. & Peplies, J. 1998 Covalent DNA–streptavidin conjugates as building blocks for novel biometallic nanostructures. *Angew. Chem. Int. Ed.* **37**, 2265–2268. (doi:10.1002/(SICI)1521-3773(19980904)37:16%3C2265::AID-ANIE2265%3E3.0.CO;2-F)

Niemeyer, C. M., Ceyhan, B., Gao, S., Chi, L., Peschel, S. & Simon, U. 2001 Site-selective immobilization of gold nanoparticles functionalized with DNA oligomers. *Coll. Polym. Sci.* **279**, 68–72. (doi:10.1007/s003960000429)

Niemeyer, C. M., Ceyhan, B., Noyong, M. & Simon, U. 2003 Bifunctional DNA–gold nanoparticle conjugates as building blocks for the self-assembly of cross-linked particle layers. *Biochem. Biophys. Res. Commun.* **311**, 995–999. (doi:10.1016/j.bbrc.2003.10.103)

Niidome, T., Yamagata, M., Okamoto, Y., Akiyama, Y., Takahashi, H., Kawano, T., Katayama, Y. & Niidome, Y. 2006 PEG-modified gold nanorods with a stealth character for *in vivo* applications. *J. Control. Release* **114**, 343–347. (doi:10.1016/j.jconrel.2006.06.017)

Noyong, M., Gloddek, K., Mayer, J., Weirich, Th. & Simon, U. 2007*a* *cis*-Pt mediated assembly of gold nanoparticles on DNA. *J. Cluster Sci.* **18**, 193–204. (doi:10.1007/s10876-006-0095-4)

Noyong, M., Blech, K., Rosenberger, A., Klocke, V. & Simon, U. 2007*b* In situ nanomanipulation system for electrical measurements in SEM. *Meas. Sci. Technol.* **18**, N84–N89.

Ofir, Y., Samanta, B. & Rotello, V. M. 2008 Polymer and biopolymer mediated self-assembly of gold nanoparticles. *Chem. Soc. Rev.* **37**, 1814–1825. (doi:10.1039/b712689c)

Okazaki, S. & Moers, J. 2005 Lithography. In *Nanoelectronics and information technology* (ed. R. Waser), pp. 221–247, 2nd edn. Weinheim, Germany: Wiley-VCH.

Pan, Y., Neuss, S., Leifert, A., Fischler, M., Wen, F., Simon, U., Schmid, G., Brandau, W. & Jahnen-Dechent, W. 2007 Size-dependent cytotoxicity of gold nanoparticles. *Small* **3**, 1941–1949. (doi:10.1002/smll.200700378)

Pan, Y., Leifert, A., Ruau, D., Neuss, S., Bornemann, J., Schmid, G., Brandau, W., Simon, U. & Jahnen-Dechent, W. 2009 Gold nanoparticles of diameter 1.4 nm trigger necrosis by oxidative stress and mitochondrial damage. *Small* **5**, 2067–2076. (doi:10.1002/smll.200900466)

Panyala, N. R., Peña-Méndez, E. M. & Havel, J. 2009 Gold and nano-gold in medicine: overview, toxicology and perspectives. *J. Appl. Biomed.* **7**, 75–91.

Park, S. Y., Lytton-Jean, A. K. R., Lee, B., Weigand, S., Schatz, G. C. & Mirkin, Ch. A. 2008 DNA-programmable nanoparticle crystallization. *Nature* **451**, 553–556. (doi:10.1038/nature06508)

Pecharromán, C., Pérez-Juste, J., Mata-Osoro, G., Liz-Marzán, L. M. & Mulvaney, P. 2008 Redshift of surface plasmon modes of small gold rods due to their atomic roughness and end-cap geometry. *Phys. Rev. B* **77**, 035418. (doi:10.1103/PhysRevB.77.035418)

Periyasamy, G. & Remacle, F. 2009 Ligand and solvation effects on the electronic properties of Au_{55} clusters: a density functional theory study. *Nano Lett.* **9**, 3007–3011. (doi:10.1021/nl901430k)

Peterle, T., Leifert, A., Timper, J., Sologubenko, A., Simon, U. & Mayor, M. 2008 Multidentate thioether ligands coating gold nanoparticles. *Chem. Commun.* 3438–3440. (doi:10.1039/b802460j)

Pileni, M. 2003 The role of soft colloidal templates in controlling the size and shape of inorganic nanocrystals. *Nat. Mater.* **2**, 145–150. (doi:10.1038/nmat817)

Pileni, M. P. 2007 Control of the size and shape of inorganic nanocrystals at various scales from nano to macrodomains. *J. Phys. Chem. C* **111**, 9019–9038. (doi:10.1021/jp070646e)

Pina, C. D., Falletta, E., Prati, L. & Rossi, M. 2008 Selective oxidation using gold. *Chem. Soc. Rev.* **37**, 2077–2095. (doi:10.1039/b707319b)

Podsiadlo, P., Sinani, V. A., Bahng, J. H., Kam, N. W., Lee, J. & Kotov, N. A. 2008 Gold nanoparticles enhance the anti-leukemia action of a 6-mercaptopurine chemotherapeutic agent. *Langmuir* **24**, 568–574. (doi:10.1021/la702782k)

Reismann, M., Bretschneider, J., von Plessen, G. & Simon, U. 2008 Reversible photothermal melting of DNA in DNA–gold–nanoparticle networks. *Small* **4**, 607–610. (doi:10.1002/smll.200701317)

Remacle, F. & Levine, R. D. 2001 Quantum dots as chemical building blocks: elementary theoretical considerations. *Chem. Phys. Chem.* **2**, 20–36. (doi:1002/1439-7641(20010119)2:1%3C20::AID-CPHC20%3E3.0.CO;2-R)

Richards, R., Bönnemann, H. C. S. S. R. & Kumar, J. H. 2005 *Nanofabrication towards biomedical applications: techniques, tools, applications, and impact.* Weinheim, Germany: Wiley-VCH.

Rosi, N. L. & Mirkin, Ch. A. 2005 Nanostructures in biodiagnostics. *Chem. Rev.* **105**, 1547–1562. (doi:10.1021/cr030067f)

Rosi, N. L., Giljohann, D. A., Thaxton, C. S., Lytton-Jean, A. K., Han, M. S. & Mirkin, Ch. A. 2006 Oligonucleotide-modified gold nanoparticles for intracellular gene regulation. *Science* **312**, 1027–1030. (doi:10.1126/science.1125559)

Rozkiewicz, D. I., Gierlich, J., Burley, G. A., Gutsmiedl, K., Carell, T., Ravoo, B. J. & Reinhoudt, D. N. 2007 Transfer printing of DNA by 'click' chemistry. *ChemBioChem* **8**, 1997–2002. (doi:10.1002/cbic.200700402)

Sardar, R. & Shumaker-Parry, J. S. 2009 9-BBN induced synthesis of nearly monodisperse ω-functionalized alkylthiol stabilized gold nanoparticles. *Chem. Mater.* **21**, 1167–1169. (doi:10.1021/cm802942x)

Sato, T., Ahmed, H., Brown, D. & Johnson, B. F. H. 1997 Single electron transistor using a molecularly linked gold colloidal particle chain. *J. Appl. Phys.* **82**, 696. (doi:10.1063/1.365600)

Schmid, G. 1985 Developments in transition metal cluster chemistry: the way to large clusters. *Struct Bonding* (*Berlin*) **62**, 51–85.

Schmid, G. 1998 The role of big metal clusters in nanoscience. *J. Chem. Soc. Dalton Trans.* 1077–1082. (doi:10.1039/a708447a)

Schmid, G. 2004 *Nanoparticles—from theory to applications.* Weinheim, Germany: Wiley-VCH.

Schmid, G. 2008 The relevance of shape and size of Au_{55} clusters. *Chem. Soc. Rev.* **37**, 1909–1930. (doi:10.1039/b713631p)

Schmid, G. & Simon, U. 2005 Gold nanoparticles: assembly and electrical properties in 1–3 dimensions. *Chem. Commun.* **6**, 697–710. (doi:10.1039/b411696h)

Schmid, G., Boese, R., Pfeil, R., Bandermann, F., Mayedr, S., Calis, G. H. M. & van der Velden, J. W. A. 1981 $Au_{55}[P(C_6H_5)_3]_{12}CI_6$ —ein Goldcluster ungewöhnlicher Größe. *Chem. Ber.* **114**, 3634. (doi:10.1002/cber.19811141116)

Schmid, G., Lehnert, A., Kreibig, U., Damczyk, Z. A. & Belouschek, P. 1990 Synthese und elektonenmikroskopische Untersuchung kontrolliert gewachsener, ligandstabilisierter Goldkolloide sowie theoretische Überlegungen zur Oberflächenbelegung durch Kolloide. *Z. Naturforsch. B* **45b**, 989–994.

Schmid, G., Pugin, R., Sawitowski, T., Simon, U. & Marler, B. 1999 Transmission electron microscopic and small angle X-ray diffraction investigations of $Au_{55}(PPh_3)_{12}Cl_6$ microcrystals. *Chem. Commun.* **14**, 1303–1304. (doi:10.1039/a902741f)

Schmid, G., Liu, Y.-P., Schumann, M., Raschke, T. & Radehaus, C. 2001 Quasi one-dimensional arrangements of $Au_{55}(PPh_3)_{12}Cl_6$ clusters and their electrical properties at room temperature. *Nano Lett.* **1**, 405. (doi:10.1021/nl0100419)

Schmid, G. *et al.* 2006 *Nanotechnology. Assessment and perspectives.* Berlin, Germany: Springer-Verlag.

Schmid, G. *et al.* 2008 Generation and electrical contacting of gold quantum dots. *Coll. Polym. Sci.* **286**, 1029. (doi:10.1007/s00396-008-1866-2)

Schön, G. & Simon, U. 1995*a* A fascinating new field in colloid science: small ligand-stabilized metal clusters and possible application in microelectronics. *Coll. Polym. Sci.* **273**, 101–117. (doi:10.1007/BF00654007)

Schön, G. & Simon, U. 1995*b* A fascinating new field in colloid science: small ligand-stabilized metal clusters and their possible application in microelectronics. Part II. Future directions. *Coll. Polym. Microelectron. Sci.* **273**, 202–218. (doi:10.1007/BF00657826)

Schulz-Dobrick, M., Srathy, K. V. & Jansen, M. 2005 Surfactant-free synthesis and functionalization of gold nanoparticles. *J. Am. Soc.* **127**, 12 816–12 817. (doi:10.1021/ja054734t)

Seferos, D. S., Giljohann, D. A., Hill, H. D., Prigodich, A. E. & Mirkin, Ch. A. 2007 Nano-flares: probes for transfection and mRNA detection in living cells. *J. Am. Chem. Soc.* **129**, 15 477–15 479. (doi:10.1021/ja0776529)

Sendrouiu, I. E., Mertens, S. F. L. & Schiffrin, D. 2006 Plasmon interactions between gold nanoparticles in aqueous solution with controlled spatial separation. *Phys. Chem. Chem. Phys.* **8**, 1430–1436. (doi:10.1039/b518112g)

Simon, U. 1998 Charge transport in nanoparticle arrangements. *Adv. Mater.* **10**, 1487. (doi:10.1002/(SICI)1521-4095(199812)10:17%3C1487::AID-ADMA1487%3E3.0.CO;2-W)

Simon, U., Schön, G. & Schmid, G. 1993*a* Die Verwendung von Au_{55}-Clustern als Quantenpunkte. *Angew. Chem.* **105**, 264–267. (doi:10.1002/ange.19931050216)

Simon, U., Schön, G. & Schmid, G. 1993*b* The application of Au_{55} clusters as quantum dots. *Angew. Chem. Int. Ed.* **32**, 250–254. (doi:10.1002/anie.199302501)

Simon, U., Flesch, R., Wiggers, H., Schön, G. & Schmid, G. 1998 Chemical tailoring of the charging energy in metal cluster arrangements by use of bifunctional spacer molecules. *J. Mater. Chem.* **8**, 517. (doi:10.1039/a707544h)

Sperling, R. A., Gil, P. R., Zhang, F., Zanella, M. & Parak, W. J. 2008 Biological applications of gold nanoparticles. *Chem. Soc. Rev.* **37**, 1896–1908. (doi:10.1039/b712170a)

Stehr, J. *et al.* 2008 Gold nanostoves for microsecond DNA melting analysis. *Nano Lett.* **8**, 619–623. (doi:10.1021/nl073028i)

Sun, H. S., Murray, C. B., Weller, D., Folks, C. & Moser, A. 2000 Monodisperse FePt nanoparticles and ferromagnetic FePt nanocrystal superlattices. *Science* **287**, 1989–1992. (doi:10.1126/science.287.5460.1989)

Talets, A., Russier, V., Courty, A. & Pileni, M. P. 1999 Collective optical properties of silver nanoparticles organized in two-dimensional superlattices. *Phys. Rev. B* **59**, 13 350–13 358. (doi:10.1103/PhysRevB.59.13350)

Torma, V., Vidoni, O., Simon, U. & Schmid, G. 2003 Charge-transfer mechanisms between gold clusters. *Eur. J. Inorg. Chem.* **6**, 1121–1127. (doi:10.1002/ejic.200390143)

Tsoli, M., Kuhn, H., Brandau, W., Esche, H. & Schmid, G. 2005 Cellular uptake and toxicity of Au_{55} clusters. *Small* **1**, 841–844. (doi:10.1002/smll.200500104)

Turkevich, J., Stevenson, P. C. & Hiller, J. 1951 A study of the nucleation and growth processes in the synthesis of colloidal gold. *Discuss. Faraday Soc.* **11**, 55–75. (doi:10.1039/df9511100055)

Turner, M., Golovko, V., Vaughan, O., Abdulkin, P., Berenguer-Murcia, A., Tikhov, M., Johnson, B. & Lambert, R. 2008 Selective oxidation with dioxygen by gold nanoparticle catalysts derived from 55-atom clusters. *Nature* **454**, 981. (doi:10.1038/nature07194)

Uchida, K., Koga, J., Ohba, R. & Toriumi, A. 2002 Programmable single-electron transistor logic for low-power intelligent Si LSI. In *Proc. IEEE Int. Solid-States Circuits Conference, San Francisco, CA, 3–7 February 2002*, vol. 1, pp. 206–460. Piscataway, NJ: IEEE.

Ung, T., Liz-Marzán, L. M. & Mulvaney, P. 2002 Gold nanoparticle thin films. *Coll. Surf. A* **202**, 119–126. (doi:10.1016/S0927-7757(01)01083-4)

van der Molen, S. J., Liao, J., Kudernac, T., Agustsson, J. S., Bernard, L., Calame, M., van Wees, B. J., Feringa, B. L. & Schönenberger, C. 2009 Light-controlled conductance switching of ordered metal-molecule-metal devices. *Nano Lett.* **9**, 76. (doi:10.1021/nl802487j)

van der Velden, J. W. A., Vollenbroek, F. A., Bour, J. J., Beurskens, P. I., Smits, J. M. M. & Bosman, W. P. 1981*a* Gold clusters containing bidentate phosphine ligands. Preparation and X-ray structure invetigation of $[Au_5(ddpmH)_3dppm)](NO_3)_2$ and $[Au_{13}(dppmH)_6](NO)_{n^*}$. *Recl.: J. R. Neth. Chem. Soc.* **100**, 148.

van der Velden, J. W. A., Bour, J. J., Bosman, W. P. & Hoordik, J. H. 1981*b* Synthesis and *X*-ray crystal structure determination of the cationic gold cluster compound $[Au_8(PPh_3)_7](NO_3)_2$. *J. Chem. Soc. Chem. Commun.* 1218. (doi:10.1039/c39810001218)

Walter, M., Akola, J., Lopez-Acevedo, O., Jadzinsky, P. D., Calero, G., Ackerson, C. J., Whetten, R. L., Grönbeck, H. & Häkkinen, H. 2008 A unified view of ligand-protected gold clusters as superatom complexes. *Proc. Natl Acad. Sci. USA* **105**, 9157–9162. (doi:10.1073/pnas.0801001105)

Warner, M. G. & Hutchison, J. E. 2003 Linear assemblies of nanoparticles electrostatically organized on DNA scaffolds. *Nat. Mater.* **2**, 272–277. (doi:10.1038/nmat853)

Waser, R. (ed.) 2005 *Nanoelectronics and information technology*, pp. 221–247, 2nd edn. Weinheim, Germany: Wiley-VCH.

Weiss, D. N., Brokmann, X., Calvet, L. E., Kastner, M. A. & Bawendi, M. G. 2006 Multi-island single-electron devices from self-assembled colloidal nanocrystal chains. *Appl. Phys. Lett.* **88**, 143 507. (doi:10.1063/1.2189012)

Wen, F., Englert, U., Gutrath, B. & Simon, U. 2008 Crystal structure, electrochemical and optical properties of $[Au_9(PPh_3)_8](NO_3)_3$. *Eur. J. Inorg. Chem.* **2008**, 106–111. (doi:10.1002/ejic.200700534)

Whetten, R. L. *et al.* 1996 Nanocrystal gold molecules. *Adv. Mater.* **8**, 428–433. (doi:10.1002/adma.19960080513)

Wilson, R. 2008 The use of gold nanoparticles in diagnostics and detection. *Chem. Soc. Rev.* **37**, 2028–2045. (doi:10.1039/b712179m)

Wilton-Ely, J. D. E. T. 2008 The surface functionalisation of gold nanoparticles with metal complexes. *Dalton Trans.* 25–29. (doi:10.1039/b714144k)

Wirges, C. T., Timper, J., Fischler, M., Sologubenko, A. S., Mayer, J., Simon, U. & Carell, T. 2008 Gesteuerte Keimbildung bei der DNA-Metallisierung. *Angew. Chem.* **121**, 225–229. (doi:10.1002/ange.200803123)

Woehrle, G. H., Warner, M. G. & Hutchison, J. E. 2004 Molecular-level control of feature separation in one-dimensional nanostructure assemblies formed by biomolecular nanolithography. *Langmuir* **20**, 5982–5988. (doi:10.1021/la049491h)

Xiao, S., Liu, F., Rosen, A. E., Hainfeld, J. F., Seeman, N. C., Musier-Forsyth, K. & Kiehl, R. A. 2002 Selfassembly of metallic nanoparticle arrays by DNA scaffolding. *J. Nanoparticle Res.* **4**, 313–317. (doi:10.1023/A:1021145208328)

Xu, L.-P. & Chen, S. 2009 Scanning tunneling spectroscopy of gold nanoparticles: influences of volatile organic vapors and particle core dimensions. *Chem. Phys. Lett.* **468**, 222–226. (doi:10.1016/j.cplett.2008.12.013)

Zabet-Khosousi, A. & Dhirani, A.-A. 2008 Charge transport in nanoparticle assemblies. *Chem. Rev.* **108**, 4072–4124. (doi:10.1021/cr0680134)

Zhang, H., Schmid, G. & Hartmann, U. 2003 Reduced metallic properties of ligand-stabilized small metal clusters. *Nano Lett.* **3**, 305–307. (doi:10.1021/nl0258980)

Zhang, X., Guo, Q. & Cui, D. 2009 Recent advances in nanotechnology applied to biosensors. *Sensors* **9**, 1033–1053. (doi:10.3390/s90201033)

Zou, B., Ceyhan, B., Simon, U. & Niemeyer, C. M. 2005 Self-assembly of crosslinked DNA–gold nanoparticle layers visualized by *in-situ* scanning force microscopy. *Adv. Mater.* **17**, 1643–1647. (doi:10.1002/adma.200402037)